博士論文

論文題目

Analysis of pharyngeal arch patterning by Hox and Dlx genes: evolutionary and developmental implication for vertebrates craniofacial morphogenesis

（Hox/Dlx遺伝子による咽頭弓のパターニングの解析：脊椎動物の頭頚部形態形成に対する進化発生学的な示唆）

氏　　名　　北沢　太郎

Analysis of pharyngeal arch patterning by Hox and Dlx genes: evolutionary and developmental implication for vertebrates craniofacial morphogenesis

(Hox/Dlx 遺伝子による咽頭弓のパターニングの解析: 脊椎動物の頭頚部形態形成に対する進化発生学的な示唆)

東京大学大学院医学系研究科分子細胞生物学専攻

指導教員：栗原裕基教授

申請者：北沢太郎

Table of Contents

Abstract

Pharyngeal Arches (PAs) are segmental structures characteristic of the pharyngula stage of vertebrates. PAs are colonized by neural crest cells (NCCs), migratory multipotent progenitors arising from the anterior dorsal neural tube. Cranial neural crest cells (CNCCs), which originate from forebrain to hindbrain levels of the neural tube, give rise to most skeletal elements of the head. The anterior-posterior (AP) identity of each PAs is specified by the combination of *Hox* genes it expresses. The first PA (PA1) is *Hox*-negative, whereas the second and third PAs (PA2 and PA3) are specified by *Hoxa2* and *Hoxa3*, respectively. In contrast to patterning along the AP axis, their dorsoventral (DV) identity is, at least in part, specified by the *Dlx*-code. The maxillary process, the dorsal part of PA1, is specified by *Dlx1/Dlx2*, whereas the mandibular process, the ventral part of PA1, is mainly specified by *Dlx5/Dlx6.* Despite extensive studies on these homeobox genes in various species, the molecular mechanisms underlying their capacity to topologically specify the body plan remain unsolved. In this paper I analyzed the function of *Hox* and *Dlx* genes in CNCCs utilizing various *Hox*- and *Dlx*-related mutant mice, and dissected their crosstalk in PAs patterning. Through rewriting experiments of the *Hox*- and *Dlx*- codes in PAs, I also revealed developmental and

evolutionary origins of the styloid process and tympanic membrane, providing new interpretation of the evolution of the mammalian middle ear.

Materials and Methods

Mice. Mice carrying the *Ednra*$^{-}$ [1], *Edn1*$^{-}$ [2], *Dlx5/6*$^{-}$ [3], *Ednra*^{Edn1} [4] and *Ednra*^{dHand} [4] allele have been previously described, maintained on a mixed C57BL/6J_ICR_129 background. To obtain mice carrying *ROSA*$^{CAG\text{-}flox\text{-}Hoxa2/+}$ allele, I inserted a cassette consisted of HCMVIEE, CAG promoter, *loxP-neo-loxP* and AU5-tagged *Hoxa2* into *pROSA26-1* (P. Soriano, Mount Sinai School of Medicine, New York, NY, USA) (addgene, plasmid 21714). I introduced this cassette into *ROSA26* locus of mouse ES cells by homologous recombination. The targeting vector was linearized and electroporated into B6129F1- derived ES cell line ATOM1 (Amano et al., unpublished). Targeted ES clones were injected into ICR blastocysts to generate chimeras. To obtain mice carrying the *ROSA*$^{CAG\text{-}flox\text{-}Hoxa2/+}$ allele, chimeras were crossed with ICR females. *ROSA*$^{CAG\text{-}flox\text{-}Hoxa2/+}$ mice were crossed with *Wnt1::Cre* mice [5] to induce NCCs-specific over-expresion of *Hoxa2* (NCC-*Hoxa2* mice) (Figure 2). To obtain NCC-*Hoxa2* mice with *Ednra*-null allele (NCC-*Hoxa2; Ednra*$^{GFP/GFP}$ mice), I crossed *ROSA*$^{CAG\text{-}flox\text{-}Hoxa2/+}$*;* *Ednra*$^{GFP/+}$ mice with *Wnt1::Cre*; *Ednra*$^{GFP/+}$ mice.

To obtain mice carrying the *Ednra*^{Hoxa2} (*Hoxa2*-knock-in) or *Ednra*^{Hoxa3} (*Hoxa3*-knock-in) allele, I performed RMCE on the *Ednra*$^{neo/-}$ ES cells, in which an

exchangeable floxed site was introduced into the *Ednra* locus as previously described [6]. Briefly, PCR-amplified fragments encoding the ORF of mouse *Hoxa2* and *Hoxa3* cDNA were introduced into the knock-in vector p66–2272 containing multiple cloning sites between *lox66* and *lox2272* [7]. 5' terminal knocked-in Hoxa2 and Hoxa3 were tagged by AU5 epitope. The resultant plasmids were transfected into $Ednra^{neo/-}$ ES cells with Cre-expressing adenovirus [8](Figure 10). Targeted ES clones were injected into ICR blastocysts to generate chimeras. As this procedure generates a dominant lethal mutation I injected recombinant ES cells into ICR blastocysts and analyzed the resulting chimeras. Highly chimeric embryos showed severe craniofacial defects and perinatal lethality. Only chimeras with low ES contribution grew normally. I eventually succeeded to generate a viable *Hoxa3*-knock-in chimeric mouse with ES cell contribution to germline. This founder enabled me to obtain and analyze heterozygous ($Ednra^{Hoxa3/+}$) embryos. As for *Hoxa2*-knock-in ES cells, I could not obtain live chimeric mice with germline contribution of ES cells. Therefore, I analyzed phenotypes caused by *Hoxa2*-knock-in in chimeric mice. To obtain $Ednra^{Hoxa3/GFP}$ mice, I crossed $Ednra^{Hoxa3/+}$ chimeras with $Ednra^{GFP/+}$ females.

Mice were housed in an environmentally controlled room at 23±2 °C, with a relative humidity of 50–60% and under a 12-h light:12-h dark cycle.

Fertilized Hojuran chicken (*Gallus gallus*) eggs were obtained from Shiroyama Keien Farms (Tochigi, Japan), and were incubated in a humidified atmosphere at 37 °C until the embryos reached appropriate stages.

All of the animal experiments were performed in accordance with the guidelines of the University of Tokyo Animal Care and Use Committee.

Skeletal Staining. Alizarin red/alcian blue staining was performed, as previously described [9]. Samples were fixed in 95% ethanol for one week, placed in acetone for two days and incubated with 0.015% alcian blue 8GS, 0.005% alizarin red S and 5 acetic acid in 70% ethanol for three days. After washing in distilled water, the samples were cleared in 1% KOH for several days and in 1% KOH glycerol series until surrounding tissues turned transparent. The specimens were stored in glycerol.

Histological analysis. The method has been described previously [10]. Each paraffin-embedded section (12 μm) was stained by hematoxyline and eosin. For three-dimensional reconstruction, digital images of the stained sections were loaded into Amira (Visage Imaging, Inc.) with a voxel size appropriate to section thickness. Images were aligned and concerned regions were labelled. The labels were resampled to

iso-volumetric voxel dimensions, and these smoothed data sets were transformed into a surface by triangulation. The number of triangles was reduced using the SmoothSurface module of Amira.

In Situ Hybridization. Whole-mount in situ hybridization was performed as described previously [11]. Probes for Six2 were generously provided by G. Oliver (St Jude Children's Research Hospital, Memphis, TN, USA). Other probes were prepared by RT-PCR.

Plasmid Construction. (PRS-1/-4)3-Luc is described previously [12]. Promoter region of Mouse Meox1 which contains Hox responsive elements [13] is cloned by PCR from mouse genome using forward primer (5'-AAGCTTCAAGGACTTTAAGAGCC-3') and reveres primer (5'-GCACGGAGTTGTTTCCTACC-3'). Mouse *Hoxa2*, *Hoxa3, Dlx2* and *Dlx5* were amplified by PCR from mouse embryo cDNA. *Hoxa2, Hoxa3, Dlx2* and *Dlx5* cDNAs were cloned into the 3' cloning sites of the epitope-tagged expression vectors pCEFL-AU5 [14].

Luciferase Assay and Western Blotting. Expression constructs, reporter constructs,

and pRL-SV40 (Promega) were co-transfected into P19 cells. Forty-eight hours after transfection, luciferase units in the cell lysates were determined with a luminometer. Transfection efficiency was normalized on the basis of Renilla luciferase activity. After luciferase assay, the rest of cell lysate was used for Western blotting. The procedure of Western blotting is described previously[12].

Transcript Profiling. The maxillary process, the mandibular process and the PA2 were dissected from E10.5 wild-type and NCC-*Hoxa2*. For the analysis of NCC-*Hoxa2;* mice, single microarray experiments were performed for wild-type and NCC-*Hoxa2* littermates. Preparation of the cRNA and hybridization of the probe arrays were performed according to the manufacturer's instructions (Affymetrix, Santa Clara, CA). Affymetrix Genechip Mouse 430 2.0 arrays containing 45,101 probe sets were applied. The expression value for each mRNA was obtained by the Robust Multi-array Analysis (RMA) method. To analyze the expression data at the genetic level, the intensity of the signal values was summarized using Entrez Gene ID (normalized to the 75th percentile). Then the gene set probes were filtered on an expression (20.0 – 100.0) percentile. The genes, which were expressed at lower than the 20 percentile in all of the four arrays were eliminated from the analyses. After excluding the gene set probes which did not

have gene symbols, about 20,000 genes remained and they were used for further analysis. Annotation of the probe numbers and targeted sequences are shown on the Affymetrix web page. Transcript profiling of wild-type and *Dlx5/6*$^{-/-}$ mice are obtained previously[15].

Ontology Analysis. I performed functional clustering using Database for Annotation, Visualization, and Integrated Discovery (DAVID) (http://david.abcc.ncifcrf.gov/).

Pharmacological inactivation of *Edn1* signaling *in ovo*. The method has been described previously [10,16]. Thirty microlitre olive oil drop was introduced onto the shell membrane at 48 h of incubation. At day 12, embryos were collected. In the bosentan-treated group, bosentan (Actelion, Ltd) was suspended in the oil at the 5mg/m1, whereas only oil was given to the control group. Totally more than ten specimens were analyzed by the three dimensional reconstruction of serial sections.

Part 1:

Partial craniofacial re-patterning induced by *Hoxa2* expression in neural crest cells: crosstalk with the *endothelin1-Dlx5/6* pathway

Summary

During early craniofacial development, cranial neural crest cells (CNCC) colonize the pharyngeal arches (PAs) and give rise to most craniofacial skeletal components. The expression profile of different members of the *Hox* and *Dlx* gene families defines, along the rostrocaudal and dorsoventral axes respectively, the capacity of CNCC to generate specific elements of the head skeleton. For example, the first PA (PA1) is *Hox*-negative, whereas the second and third PAs (PA2 and PA3) are specified respectively by *Hoxa2* and *Hoxa3*. Little is known about the *Hox*/*Dlx* interaction during PA patterning and morphogenesis. Here I show that ectopic expression of *Hoxa2* in all *Hox*-negative CNCCs results in distinct phenotypes, depending on the *Dlx* expression pattern of specific CNCC subpopulations. Namely, *Hoxa2* expression results in the morphological and molecular transformation of proximal elements of PA1, into PA2-like structures with duplication of the hyoid cartilage and styloid process. Distal elements of PA1, are less affected, but become severely hypomorphic on a *Dlx5/6*-knock down background. Over-expression of *Hoxa2* also prevents differentiation of CNCC-derived components of the skull where *Dlx* genes are not expressed. Transcriptome profiling provides further support to the notion of a Hox/Dlx crosstalk in defining craniofacial

morphogenesis. These results provide a conceptual framework to reconcile previous results and bring novel insights on anteroposterior/dorsoventral interactions during patterning of the head.

Introduction

Hox genes are evolutionary conserved master regulators of morphogenesis [17-20]. In vertebrates, they specify the anterior-posterior (AP) identity of pharyngeal arches (PAs) and somites, and the proximal-distal (PD) identity of limbs. Unveiling the functions of *Hox* genes is central to understand the origin of the animal body plan. Despite extensive studies on *Hox* genes in various species, the molecular mechanisms underlying their capacity to topologically specify the body plan remain unsolved.

PAs are segmental structures characteristic of the pharyngula stage of vertebrates. PAs are colonized by neural crest cells (NCCs), migratory multipotent progenitors arising from the anterior dorsal neural tube, and by mesodermal cells. Cranial neural crest cells (CNCCs), which originate from forebrain to hindbrain levels of the neural tube, give rise to most skeletal elements of the head while craniofacial muscles derive from mesodermal cells. The AP identity of each PA is specified by the combination of *Hox* genes it expresses [21,22]. PA1 is *Hox*-negative, whereas the second and third PAs (PA2 and PA3) are specified by *Hoxa2* [23,24] and *Hoxa3* [25], respectively (Figure 1). Inactivation of *Hoxa2* results in the homeotic transformation of PA2 into PA1-like structures [23,24]. Furthermore, conditional inactivation of *Hoxa2* resulted in the same PA2 to PA1-like transformation [26], indicating that the expression of *Hoxa2* in CNCCs

is essential for PA2 specification.

By contrast, it remains unclear whether *Hox* genes can operate the genetic program that specifies regional identities autonomously in CNCCs. Ectopic expression of *Hoxa2* in the *Hox*-negative region induced partial transformation of PA1 into PA2-like structures [27,28], whereas other studies have shown that ectopic expression of *Hoxa2* results in deterioration of skull and face development without transformation [28-30]. It has been unsolved how to reconcile these two incompatible phenotypes induced by ectopic *Hoxa2* in PAs. Although some findings suggest that other cell types surrounding CNCCs may need to express *Hoxa2* for PA2 specification [28-30], no definite answer has been given to this issue.

Another unsolved issue concerning PA development is how patterning programs along different axes are integrated in CNCCs. In contrast to patterning along the AP axis, their dorsoventral (DV) identity is, at least in part, specified by the *Dlx*-code [22,31]. The maxillary process, the dorsal part of PA1, is specified by *Dlx1/Dlx2*, whereas the mandibular process, the ventral part of PA1, is mainly specified by *Dlx5/Dlx6* [31] (Figure 1). Indeed, inactivation of *Dlx5* and *Dlx6* [3,31] or of their upstream inducers endothelin-1 (Edn1) and endothelin receptor type-A (Ednra) [2,32,33] results in the transformation of the mandibular into a maxillary-like process. In posterior PAs *Hox*

and *Dlx* genes are simultaneously expressed in CNCCs, and might cooperate in defining craniofacial morphogenesis [34], but hitherto no experiments have been performed to dissect possible crosstalk between *Hox* and *Dlx* genes in PA patterning.

To address these issues, I have altered the *Hox*-code in the head by conditionally over-expressing *Hoxa2* in *Hox*-negative CNCCs which give rise to the PA1 and frontonasal derivatives. I observe distinct phenotypes, depending on the specific CNCC subpopulations over-expressing *Hoxa2*. Namely, the expression of *Hoxa2* in PA1 CNCCs induces a partial PA1-to-PA2 transformation, indicating that *Hoxa2* is not only necessary but also sufficient for PA2 specification. In addition, ectopic *Hoxa2* and *Hoxa3* also similarly induced a hypoplastic phenotype of craniofacial structures originated from midbrain and forebrain CNCCs, in consistent with previous results in the chick[28,29]. These two types of apparently incompatible phenotypes correspond to subpopulations of *Hox*-negative CNCCs of different origins. Importantly, I found that *Hoxa2* and *Dlx5/6* genes coordinately pattern the styloid process, whereas *Dlx5/6* prevents the hypoplastic phenotype induced by ectopic *Hoxa2*. Thus, present study has reconciled the conundrum on the effect of *Hoxa2* on CNCC specification and has further revealed crosstalk between *Hox* and *Dlx* genes that contributes to PA patterning.

Results

Skeletal defects resulting from ectopic expression of *Hoxa2* in CNCCs

To induce ectopic expression of *Hoxa2* in the *Hox*-negative contingent of CNCCs which migrate to the PA1 and to the frontonasal eminence, I generated $ROSA^{CAG\text{-}flox\text{-}Hoxa2/+}$ mice and crossed them with *Wnt1::Cre* mice to obtain *Wnt1::Cre*;$ROSA^{CAG\text{-}flox\text{-}Hoxa2/+}$ (hereafter referred to as NCC-*Hoxa2*) mice (Figures 2A-C). I evaluated over-expression of *Hoxa2* by in situ hybridization (Figures 2D, E). These mice were characterized by a short snout, exencephaly and cleft palate (Figures 3A,D). Skeletal preparations revealed that many of the structures which normally derive from *Hox*-negative CNCCs were severely distorted or absent in NCC-*Hoxa2* mice (Figures 3B, C, E, F). Skull vault bones and maxillary structures including the frontal, squamous and jugal bones were absent or strongly reduced (Figures 3B, E, G). Skull base structures including the nasal septum, premaxillary, vomer, palatine, pterygoid, alisphenoid and maxillary bones were severely distorted (Figures 3C, F, G). The proximal part of the dentary bone, including the condylar process, was hypoplastic, whereas the distal part of the dentary was less affected (Figures 3B, E, G).

A previous study has suggested that down regulation of *FGF8* is the cause for

hypoplasia of craniofacial structures in CNCC-ablated chicks [35]. To examine whether *FGF8* is down-regulated in my mice, I performed in situ hybridization of *FGF8* at the pharyngula stage, and found that the expression of *FGF8* was not altered (Figures 4A-D), indicating that the phenotypes of *Hoxa2* over-expression were independent of *FGF8*.

CNCC-specific ectopic expression of *Hoxa2* is sufficient for transformation of certain PA1 derivatives into PA2-like structures

In addition to the phenotypes described above, conditional ectopic expression of *Hoxa2* in CNCCs resulted in striking morphological changes suggesting homeotic transformation of certain CNCC-derived PA1 structures into PA2-like derivatives. For instance, proximal PA1-derivatives including the malleus, the incus, the ectotympanic process, the gonial, pterygoid and squamous bones were absent; at their place I found duplications of skeletal structures resembling PA2-like derivatives such as the stapes, the styloid process, the lesser horn and the hyoid body (Figures 3J-L). Distal PA1 derivatives including a large part of the Meckel's cartilage and of the dentary bone were still present although smaller and malformed (Figures 3E, G). As in the case of *Hoxa2* knock-out mice (Gendron-Maguire et al., 1993; Rijli et al., 1993), this transformation

displayed a mirror-image pattern with the orthotopic PA2-derivatives across the PA1-PA2 boundary (Figure 3L). Moreover, the auricle was also duplicated (and, in some cases, even triplicated) in NCC-*Hoxa2* mice (Figures 5A-C), suggesting that this structure may also be normally mainly derived from PA2 CNCCs, whereas the external acoustic meatus was absent (Figures 3H, I).

CNCC-specific over-expression of *Hoxa2* affects muscle patterning and connections in the head.

Craniofacial muscles of NCC-*Hoxa2* mice were examined by three-dimensional reconstruction. The lingual hyoglossal-like muscle was connected to both the normal and ectopic hyoid bones (Figures 3M, N). The styloglossal-like muscle was connected to the ectopic styloid process, while the normal styloid process did not present any muscle attachment (Figures 3O, P). The ectopic styloid process and hyoid bone, but not their normal counterparts, were connected by a stylohyal-like muscle (Figures 3O, P). These results suggest that, even if *Hoxa2* expression is not induced in the mesodermal lineage, transformations of skeletal structures can induce ectopic attachment sites of pharyngeal muscles. I also observed abnormal connection of muscles between the angular process and the geni apophysis (Figures 3Q, R), which might be interpreted as a

misconnection of the genihyoid muscle or of the anterior belly of the digastric muscle. The masseter and pterygoid muscles were found to connect the dentary bone with ectopic cartilages below the cranial base (Figures 3Q, R).

CNCC-specific expression of *Hoxa2* re-patterns PA1 into PA2-like gene expression profiles

I then examined by in situ hybridization the gene expression pattern of *Pitx1*, *Msx1* and *Six2* in NCC-*Hoxa2* mice. The typical expression patterns observed in PA1 were transformed into those usually present in PA2 (Figures 6A-F). Namely, PA1-specific expression of *Pitx1* and *Six2* was down-regulated (Figures 6D, F), whereas *Msx1* expression, which is usually observed in PA2, was detected in PA1 as a mirror image across the PA1-PA2 boundary (Figures 6E). To better characterize the PA1 to PA2 transformation, I performed a transcriptome analysis on PA1 and PA2 from E10.5 wild-type and NCC-*Hoxa2* mice. The maxillary and mandibular processes were analyzed separately and their identity was confirmed according to the presence or absence of *Dlx5/6* expression. I therefore analyzed six sample groups with distinct *Hoxa2* and *Dlx5/6* expression profiles (Figures 6G, 7). The expression of *Pitx1* and *Six2* was down-regulated in the PA1 of NCC-*Hoxa2* mice. Ontology analysis showed that

many deregulated genes were categorized as transcription factors that regulate embryonic processes such as positional specification and NCC differentiation (Figure 7), supporting the validity of my microarray analysis.

To analyze the overall effect of *Hoxa2* on PA1 transcriptional profile, I performed a fractional analysis. I categorized genes into six groups according to differences in expression levels between the NCC-*Hoxa2* and wild-type maxillary process (Figure 6H, horizontal axis (d/a)) or mandibular process (Figure 6I, horizontal axis (e/b)), and stratified each group into six subgroups according to expression difference comparing the PA2 and maxillary process (Figure 6H, vertical axis (c/a)) or the mandibular process of wild-type mice (Figure 6I, vertical axis (e/b)). This analysis shows that, after transformation, the PA1 expression profile had become similar to that of the PA2. Notably, more genes were affected by ectopic *Hoxa2* in the maxillary process than in the mandibular process, suggesting that the effect of *Hoxa2* was stronger in the maxillary than in the mandibular process (Figures 13A, B). I also compared the transcriptome of NCC-*Hoxa2* PA1 with previously published profiling results of *Hoxa2*-knock-out PA2 [36], and confirmed that these two datasets show opposite changes in gene expression profile (Figure 7). Furthermore, I referenced ChIP-seq data for *Hoxa2* [36], and found that many direct targets of *Hoxa2* are strongly deregulated by

Hoxa2 over-expression in the PAs (Figure 7).

Hoxa2 and _Dlx5/6_ genetically interact and are both necessary for styloid process morphogenesis

The above molecular and morphological data support a fundamental role of *Hoxa2* in conferring PA2 identity to CNCCs. However, it is still unclear how this *Hoxa2* dependent rostrocaudal program may locally integrate the *Dlx* dependent program to pattern PA2 structures along the dorsoventral axis. I focused on the morphogenesis of the styloid process, a PA2 mammalian-specific element providing the anchor for some cranial muscles and ligaments, and analysed this structure in $Dlx5/6^{-/-}$ and $Ednra^{GFP/GFP}$ mice, in which *Dlx5* and *Dlx6* are down-regulated [6]. In both $Dlx5/6^{-/-}$ and $Ednra^{GFP/GFP}$ homozygous mutant mice, the styloid process was distally truncated (Figures 8A, B), indicating that the *endothelin-Dlx5/6* pathway is necessary for the proper generation of the styloid process in PA2. Indeed, when *Hoxa2* was over-expressed in *Hox*-negative PA1 CNCCs in the context of a *Dlx5/6*-knock down (NCC-$Hoxa2;Ednra^{GFP/GFP}$ mice), the duplicated styloid process was also distally truncated (Figures 8C, D), indicating that both *Hoxa2* and *Dlx5/6* are normally necessary to coordinate normal patterning of the styloid process in ventral PA2.

The hypoplastic phenotype induced by ectopic expression of *Hox* genes in CNCCs is more severe in dorsal structures

As observed for the NCC-*Hoxa2* mice, there was a remarkable gradient of severity in the phenotype observed in structures derived from different CNCC contingents. The most severely impaired were pre-pharyngeal components, such as the frontal bone, which were absent; maxillary process components such as the maxillary and palatine bones were severely impaired, but still present. By contrast, mandibular derivatives were almost intact or modestly affected. Overall, the severity of the phenotype seems to present an inverse correlation with the level of expression of *Dlx* genes: CNCC contingents which present high levels of *Dlx* expression such as those colonizing the PA1 mandibular process are less affected by *Hox* over-expression (Figure 9). I also analyzed craniofacial hypoplasia induced by ectopic expression of *Hoxa2* and *Hoxa3* in cranial neural crest cells including *Hox*-negative contingents under *Ednra* promoter [6] (*Ednra*$^{Hoxa2/+}$ *and Ednra*$^{Hoxa3/+}$ respectively) (Figure 10). Although phenotype were milder compared with NCC-*Hoxa2*, I also found the same inverse correlation with the level of expression of *Dlx* genes (Figure 9).

The difference in phenotypic severity between maxillary and mandibular

structures led me to speculate that the effect of ectopic *Hox* genes might depend on the cellular and genetic context along the DV axis. To test this possibility, I analyzed the effect of *Hoxa2* over-expression in the *Ednra*-null mandible, which is transformed dorsally into a maxillary structure with downregulation of *Dlx5/Dlx6* genes [32,33]. In *Ednra*-null mice crossed into the conditional *Hoxa2* over-expression allele (NCC-*Hoxa2;Ednra*$^{GFP/GFP}$), the transformed mandible was much more severely affected than in the *Ednra* mutant and the squamous bone was lost, resulting in the loss of most PA1 derivatives (Figure 11). The morphology of the skull vault and base of NCC-*Hoxa2; Ednra*$^{GFP/GFP}$ mice was similar to that of NCC-*Hoxa2* mice (Figure 11). I also generated mice which over-express *Hoxa3* under the *Ednra* promoter on the *Ednra*-null mandible (*Ednra*$^{Hoxa3/GFP}$) and obtained very similar results as described above (Figure 12). Thus, these results support the hypothesis that ectopically expressed *Hox* genes have a more severe effect in a dorsal context, suggesting a possible competition with *Dlx* transcription factors, which are known to specify the DV identity.

Profiling of NCC-*Hoxa2* dorsal and ventral PA1 components suggests transcriptional competition between *Hoxa2* and *Dlx5/6*

To evaluate a possible transcriptional crosstalk between *Hox* and *Dlx* genes, I revisited

the profiling analysis of PAs from wild-type and NCC-*Hoxa2* mice described above (Figure 6A). Firstly, I analyzed the differential transcriptional effect of ectopic *Hoxa2* on distinct DV components of PA1. Namely, I analyzed about 20,000 genes by microarray and found that ectopic *Hoxa2* up- and down-regulated more than two-folds 79 and 76 genes, respectively, in the maxillary process, whereas only 27 genes and 11 genes are up- and down-regulated, respectively, by ectopic *Hoxa2* in the mandibular process (Figure 13A). Given the fundamental role played by *Dlx5/6* in defining mandibular vs. maxillary identity, these results strongly suggest that the attenuated effect of ectopic *Hoxa2* on gene expression in the PA1 mandibular, as compared to the maxillary, component may be due to the expression of *Dlx5/6* (Figure 13B).

To further analyze the effect of *Dlx5/6* on the transcriptional activity of *Hoxa2*, I categorized genes into six groups according to differences in expression levels between the NCC-*Hoxa2* and wild-type maxillary process (Figure 13C, horizontal axis (d/a)), and stratified each group into six subgroups according to expression differences associated with the additional effects of *Dlx5/6* (Figure 13C, vertical axis (e/d)). As a result, I found that the changes in expression levels tended to be smaller in the presence of *Dlx5/6* expression (Figure 13C, E). I also generated heat maps of genes up- or down-regulated more than two-folds in the maxillary process (Figure 13D, upper law),

and observed that *Dlx5/6* have distinct tendency to compete against *Hoxa2* (Figure 13D, bottom law).

Furthermore, I performed in situ hybridization at the pharyngula stage of NCC-*Hoxa2* embryos and confirmed that *Barx1* is selectively down-regulated in the maxillary process (Figures 13F, I), and *Cyp26a1* and *Meox1* are selectively up-regulated in the maxillary process (Figures 13 G, H, J, K). I also evaluated expression of *Dlx* genes in PAs by in situ hybridization and found that overall expression pattern of them were not altered (Figure 14).

These results are consistent with the inference that *Dlx5/6*-negative CNCCs are more susceptible to the effect of *Hoxa2* expression than *Dlx5/6*-positive CNCCs within PA1.

Dlx factors suppress Hox transcriptional activity on shared target genes

Next, I analysed genes that showed distinct differences in expression levels between wild-type and *Dlx5/6*$^{-/-}$ mandibular arches and found that they are likely to be direct targets of Hoxa2, as identified by ChIP-seq analysis [36] (Figure 13L). This result indicates that Hoxa2 and Dlx5/6 might share a number of target genes, and Dlx5/6 can interfere with Hoxa2 transcriptional activity.

I next examined the effect of Dlx transcription factors on Hox transcriptional activity using a luciferase assay in P19 embryonal carcinoma cells. First, I used the reporter plasmid *(PRS-1/-4)$_3$-Luc* [12], which contains three tandem repeats of an artificial homeobox-responsive element (Figure 13M). Hoxa2 and Hoxa3 showed strong transcriptional activity on this sequence (Figures 13N, O, P). Dlx5 and Dlx2 also activated transcription, but their activity on this sequence was much lower than Hoxa2 and Hoxa3 (Figures 13N, O, P), although the levels of Hox and Dlx proteins after transient transfection were comparable (Figure 13N). Interestingly, when Hox and Dlx proteins were coexpressed, Hox-induced luciferase activity was significantly reduced, resulting in intermediate levels between Hox-induced and Dlx-induced activities (Figures 13N, O, P).

To further confirm this Hox-Dlx interaction, I performed a luciferase assay with the *Meox1* promoter, a direct target of Hoxa2 in PA2 development [13]. The *Meox1* promoter region containing Hox-responsive elements was cloned upstream of the luciferase gene to produce the reporter plasmid *Meox1pro-Luc* (Figure 13M). Luciferase assay using this reporter plasmid revealed essentially the same results as the assay with *(PRS-1/-4)$_3$-Luc*; high and low transcriptional activity induced by Hoxa2 and Dlx5/Dlx2, respectively, and suppression of Hox-induced activity by Dlx5 and Dlx2 (Figures 13Q,

R). Consistently with the observed dorsoventral differences in the severity of the phenotype of *Hox* knock-in mice, these results indicate that Hox transcriptional activity is inversely correlated with Dlx expression levels.

Discussion

All vertebrates share a basic ground plan of craniofacial structures including the skull and PA-derived visceral skeleton [21,22]. CNCCs, an evolutionary conserved feature of vertebrates, with distinct *Hox*- and *Dlx*-codes provides a region-specific contribution to these structures [22]. In PAs, *Hox* genes are expressed in nested patterns up to PA2, and no *Hox* genes are expressed in PA1, which is therefore regarded as a *Hox*-code default state. In this study, I conditionally and ectopically expressed *Hox* genes in *Hox*-negative CNCCs and analysed their impact on craniofacial patterning in distinct *Dlx* expressing subpopulations.

Several previous studies have analyzed the effect of ectopic expression of *Hoxa2* on craniofacial morphogenesis, and have reported two disparate phenotypes. Some have shown homeotic transformation of PA1 to PA2-like structures [27,28,37], whereas others have shown that ectopic expression of *Hoxa2* is deleterious for skull and face development [28-30]. It has been unclear how to reconcile these two phenotypes, but I thought that the analysis of my NCC-*Hoxa2* mice could provide the reasonoble interpretation of them. My results indicate that CNCC-specific over-expression of *Hoxa2* is sufficient for both types of phenotypes, and furthermore these phenotypes can be explained by the differential effects of ectopic *Hoxa2* expression in distinct

subpopulations of CNCCs.

Firstly, skeletal structures of PA1 showed partial homeotic transformation into those of PA2 by CNCC-specific over-expression of *Hoxa2*. Skeletal muscles and epithelium of the external acoustic meatus, which did not express ectopic *Hoxa2*, also showed transformation. Inactivation or knock-down of *Hoxa2* in various species showed homeotic transformation of PA2 components into PA1-like structures [23,24,30,37,38], and notably, NCCs-specific inactivation of *Hoxa2* induced clear duplication of PA1 components [26] (Table 1), indicating the expression of *Hoxa2* in NCCs is necessary for specification of the PA2. On the other hand, previous studies in the chicken embryo have shown that while ectopic expression of *Hoxa2* in both CNCCs and surrounding tissues leads to homeotic transformation of PA1 into PA2, the expression of *Hoxa2* only in CNCCs is not sufficient to induce this transformation [27-29,37] (Table 1). Thus, it has been suggested that *Hox*-dependent environmental cues other than CNCCs are likely to be required for the activation of a PA2-specific genetic program [28]. In this study I show that selective expression of *Hoxa2* in CNCCs results in the appearance of PA2 derivatives within the PA1 (*Hox*-negative) context, reinforcing the notion that NCCs are master regulators of PA identity.

In contrast to the proximal part of PA1, distal PA1 derivatives of the mandibular

arch (the distal part of Meckel's cartilage and distal dentary bone) and of the maxillary arch (maxillary bone, jugal bone and palatine bone) did not undergo transformation. Correspondingly, targeted inactivation of *Hoxa2* in the mouse induced the transformation of PA2 elements into of a duplicated set of PA1-like elements normally derived from the proximal part of PA1, while the distal part of PA1 was not duplicated [23,24]. Taken together, these results show that in mice, only the proximal part of the PA1 may share a *Hox* ground state with PA2 and is therefore competent for *Hoxa2*-induced transformation. It is notable that this difference in responsiveness to ectopic *Hoxa2* corresponds to the origin of CNCCs that migrate into PA1. In amniotes, the proximal PA1 derivatives which have the competency to show transformation by ectopic *Hoxa2* are contributed by rhombomere-derived CNCCs, while the distal PA1 derivatives which only show hypoplastic phenotype by ectopic *Hoxa2* are contributed by posterior midbrain-derived CNCCs [39,40], suggesting that these two subpopulations within *Hox*-negative CNCCs may be different in terms of the competence for *Hoxa2*-induced transformation (Figure 15). Previous studies in chicken embryos showed that CNCC-specific over-expression of *Hoxa2* did not induce transformation of PA1 to PA2 and all the skeletal structures generated from *Hox*-negative CNCCs were absent [28,29]. This may be because the ectopic *Hoxa2* expression induced by the

strong promoter of RCAS may overwhelm physiological expression levels of *Hoxa2*, leading to a hypoplastic phenotype even in rhombomere-derived CNCCs. This indicates that both midbrain- and rhombomere-derived CNCCs can undergo *Hoxa2*-induced hypoplasia, but midbrain-derived contingents may be more sensitive to ectopic *Hoxa2* than rhombomere-derived ones.

In zebrafish, mis-expression of *Hox* paralogue group 2 caused the complete transformation of the Meckel's cartilage into a ceratyhyal cartilage, and near-complete transformation of the palatoquadrate into a hyomandibular [37,41]. This may be explained by the minor contribution of midbrain-derived CNCCs to PA1 in zebrafish [42] unlike in amniotes. In order to dissect the property of these midbrain-derived CNCCs which contribute to PA1 in an amniote-specific manner, it will be significant to solve what makes this difference in responsiveness to ectopic *Hoxa2* between midbrain- and forebrain-derived CNCCs. Previous studies have shown that pre-migratory *Hox*-negative CNCCs are inter-changeable, and pharyngeal endoderm endows these CNCCs with positional information [43], indicating that environmental cues from surrounding tissues may contribute to the competence of CNCCs for *Hoxa2*-induced transformation.

The present study has further revealed crosstalk between *Hox* and *Dlx* genes in PA

patterning. When I focused on the hypoplastic phenotype, I found that the severity of the craniofacial phenotype induced by *Hoxa2* over-expression was well correlated with the level of *Dlx* expression in CNCCs, and knock-down of endothelin-Dlx5/6 pathway in PAs enhanced the hypoplastic phenotype, indicating that Dlx5 and Dlx6 are likely to act preventing the effects of ectopic *Hox* genes both at the morphological and molecular levels. On the other hand, ectopic *Hoxa2* expression in PA1 resulted in transformation of the proximal Meckel's cartilage into styloid-like structure, suggesting that *Hoxa2* and *Dlx5/6* cooperate in the formation of PA2-derived structures.

In posterior PAs, *Hox* and *Dlx* genes are co-expressed along the AP and DV axis, respectively [22,31], and it has been of interest how they simultaneously endow CNCCs with positional information [34]. The present study addressed this issue and first clearly revealed a crosstalk between *Hoxa2* and *Dlx5/6* transcriptional activities in pharyngeal arch patterning (Figure 15). Previous study revealed that Hox and Dlx are homeodomain-containing transcription factors which recognize very similar sequences with a TAAT motif *in vivo* [44]. It is conceivable that *Hox* and *Dlx* genes may recognize common target genes but regulate them differently, resulting in a complex and dynamic crosstalk. Intrinsic *Hox* and *Dlx* genes expressed in rhombomere-derived CNCCs may act synergistically in the specification of PAs derivatives. My results suggest that the

hypoplastic phenotype resulting from ectopic expression of *Hox* genes in CNCCs, may derive from an unbalance between *Hox* and *Dlx* gene regulation possibly through a competition for common responsive elements. Such a complex and dynamic regulatory network will, most probably, include other homeobox-containing transcription factors present in the cephalic region, including, for example *Pax*, *Otx, Alx* and other genes. Thus, the results shown in this chapter should be the first step to analyze the combinatorial role of homeobox-containing transcription factors to understand cell fate determination and morphogenesis during craniofacial development.

Part 2:

Evolutionary and developmental dual origins of the mammalian styloid process

Summary

Evolution of the mammalian middle ear has long been among the most formidable conundrum for comparative morphologists. Mammalian middle ear consists of three ossicles (the malleus, incus and stapes), while modern diapsids (reptiles and birds) have only one (the columella auris). Homology of middle ear ossicles between mammals and diapsids has long been intensively analyzed, and at present mammalian malleus and incus are proved to be the 1st pharyngeal arch (PA1)-derived structures and homologous to reptilian jaw skeletons, the articular and quadrate bone, respectively. Moreover, both the stapes and columella auris are considered to be evolutionary derived from the hyomandibular, the main dorsal component in PA2 of elasmobranchs. In this context, the styloid process, a mammalian-specific PA2-derived skeletal structure, has also been mainly regarded to be originated from the hyomandibular. It has been considered that the hyomandibular of ancestral tetrapods are separated into two parts to generate the mammalian stapes and styloid process. However, detailed analyses of evolutionary origin of the styloid process hitherto have not been performed. In this study I utilize several *Hox* and *Dlx* genes-related mutant mice, which show anteroposterior and dorsoventral patterning defects of PAs, respectively, and investigate

evolutionary and developmental origins of the styloid process. I reveal that the styloid process is generated from both the *Dlx5/6*-positive and –negative cranial neural crest cells, and evolutionarily originated not only from the hyomandibular but also from the ceratohyal components. These findings can strictly define the dorsoventral boundary of PA2 in mammals, and should be useful to dissect critical developmental events which accounts for the differential and unique middle ear systems among amniotes.

Introduction

The mammalian middle ear is a representative morphological feature which identifies this class of vertebrates, and the evolution of this structure has long been among the most significant issue of comparative zoology, developmental biology and paleontology for about 200 years [45,46]. Modern mammals have three middle ear ossicles (the malleus, incus and stapes), while diapsids have only one ossicle (the columella auris or stapes), and it has been intensively studied how to explain this difference. In present understanding, the mammalian stapes and diapsid culumella auris are recognized as homologous components. As for the malleus and incus, they are proved to be homologous to the reptilian articluar and quadrate bone, which form the articulation of lower- and upper jaws of diapsids [45,46]. However, developmental process and molecular mechanism that can explain these variations among amniotes remains to be solved.

Pharyngeal arches (PAs) are vertebrate-specific metameric structures that generate majority of craniofacial structures. PAs are separated along the anteroposterior axis, and each PA can be further subdivided dorsoventrally. The simplest configuration of gnathostome PAs is evident in elasmobranchs, and pharyngeal skeletons of all the

gnathostomes can be basically explained by metamorphose of this ground pattern [47]. The 1st PA (PA1, the mandibular arch) consists of lower and upper jaws, called the Meckels's cartilage and palatoquadrate, respectively, and articulation of these cartilages evolved the mammalian malleal/incal articulation as described above. On the other hand, the main ventral and dorsal components of the 2nd PA (PA2, the hyoid arch) are called the ceratohyal and hyomandibular, respectively, and the mammalian stapes and reptilian columella auris are derived from the hyomandibular [47]. To understand how amniotes evolved these distinct middle ear systems, it is undoubtedly essential to identify precise homology in PAs-derived skeletons among amniotes. However, in contrast to PA1-derived jaws, no articulation exists in mammalian PA2, and therefore it has been conundrum how to define the dorsoventral (ceratohyal/ hyomandibular) boundary in mammalian PA2.

Mammalian PA2 skeletal structures consist of the hyoid body, lesser horn, styloid process and stapes. The stylohyal ligament connects the lesser horn and styloid process. In particular, the styloid process, a mammalian-specific skeletal structure which works as an anchor for cranial muscles and ligaments, may be a key structure to understand dorsoventral regionality of PA2. Comparative morphologists indicated dorsal (hyomandibular) origin of the styloid process [47,48]. It has been considered that the

dorsal process of hyomandibular was separated from the main body in ancestral synapsids and fused to the otic capsule, and consequently the styloid process of modern mammals is generated [47,49]. Indeed, recently O'Gorman investigated the styloid process with genetic approach of mice, and proposed that whole the styloid process is derived from hyomandibular [50]. At present, the styloid process is accepted to have evolutionary and developmental dorsal origins [51-53], and the dorsoventral boundary of PA2 is supposed to exist between the styloid process and hyoid bone [50]. However, further analysis should be necessary to better understand evolution of the styloid process.

Recent progress of experimental developmental biology and molecular biology has endowed the molecular entity with the regionality of PAs. PAs-derived skeletal structures are generated from cranial neural crest cells (CNCCs), and the anteroposterior and dorsoventral positional address of CNCCs is endowed by *Hox* and *Dlx* genes, respectively [22,52]. As for *Hox* genes, PA1 is *Hox*-negative, and PA2 and PA3 is specified by *Hoxa2* and *Hoxa3*, respectively [23-25]. Indeed, inactivation of *Hoxa2* in PA2 results in homeotic transformation of PA2-derived structures into PA1-like forms [23,24,30,37,38], while ectopic expression of *Hoxa2* in PA1 conversely induces homeotic transformation of PA1-derived structures into PA2-like ones [27,28,37,54]. On

the other hand, *Dlx* genes are expressed in the nested pattern along the dorsoventral axis in each PA, and the dorsal components and ventral components are mainly specified by *Dlx1/2* and *Dlx5/6*, respectively [52,55]. Indeed in mice, inactivation of *Dlx5/6* or their upstream inducer, *Endothelin-1* (*Edn1)* and *Endothelin receptor type A* (*Ednra)*, results in homeotic transformation of the lower jaw into upper jaw [2,3,31-33], in contrast, ectopic activation of Edn1-Dlx5/6 cascade conversely induces transformation of the upper jaw into lower jaw [4]. Recent studies revealed that all the gnathostomes including elasmobranchs and mammals basically share this blue print of the "*Dlx*-code" [51,56,57].

In elasmobranchs and teleosts, dorsoventral patterning of PA2 by *Dlx* genes has been definitely clarified [51,52,58]. The *Edn1-Dlx5/6* cascade specifies the ceratohyal and ventral part of the hyomandibular, while dorsal part of the hyomandibular is specified by only *Dlx1/2*. On the other hand, in mammals, *Dlx1/2*-null mice show defects of the styloid process apparently confirming dorsal origin of this skeleton [53], but it has also been reported that *Dlx5/6* inactivation results in truncation of the styloid process [55], thus it should be essential to reconcile these apparently controversial phenotypes (Figure 16).

In this report, I analyzed phenotypes of several *Hox* and *Dlx*-related mutant mice, and re-examined evolutionary and developmental origins of the styloid process. I found that the styloid process has developmental dual origin; the distal and proximal parts of the styloid process are generated from *Edn1-Dlx5/6*-positive and -negarive CNCCs, respectively. *Hoxa2*-over-expression in PA1 revealed that the distal part of the styloid process is the serial homologue of the Meckel's cartilage, suggesting that this component is evolutionary derived from the ceratohyal. These results clarify that dorsoventral (hyomandibular/ ceratohyal) boundary of mammalian PA2 exists in the middle of styloid process, and provide new organized framework to investigate developmental process which generate clade-specific formulation of the middle ear.

Results

Inhibition Edn1-Dlx5/6 cascade in PA2 selectively affects the distal part of the styloid process.

Firstly, I inhibited Edn1-Dlx5/6 cascade in PAs and examined the phenotype of the styloid process. In *Dlx5/6*-, *Edn1*- and *Ednra*-null mice, the styloid process was distally truncated, while the most proximal part and the otic capsule remained normal (Figures 17A-H). These results suggest a possibility that Edn1-Dlx5/6 cascade is necessary for CNCCs to properly generate the distal part of the styloid process, while the proximal part is generated independently on this cascade.

To further examine dependency of the styloid process on Edn1-Dlx5/6 cascade, I utilized NCC-*Hoxa2* mice. In NCC-*Hoxa2* mice, *Hoxa2* is ectopically expressed in CNCCs which migrate to PA1, and PA1-derived skeletal structures shows homeotic transformed into PA2-like ones, resulting in the duplication of the styloid process (Figures 17I-K). Indeed, inhibition of Edn1-Dlx5/6 cascade in NCC-*Hoxa2* mice impaired proper morphogenesis of both the PA2- and PA1-derived styloid process as described above (Figure 8), however the proximal part of the styloid process was still

present (Figures 17L-N), suggesting that the distal and proximal part of styloid process may be generated by complementary developmental mechanisms.

Ectopic induction of Edn1-Dlx5/6 cascade in the dorsal PA2 results in the selective absence of the proximal part of the styloid process.

To dissect the regionality of the proximal part of the styloid process which was not affected by inhibition of Edn1-Dlx5/6 cascade, I utilized *Edn1*-over-expression (*Ednra*$^{Edn1/+}$) mice, in which ectopic *Edn1* induce aberrant expression of *Dlx5/6* in the dorsal region of PAs and the maxillary process is transformed into the mandibular identity [4]. Indeed, in contrast to inhibition of Edn1-Dlx5/6 cascade described above, aberrant induction of Edn1-Dlx5/6 cascade results in the absence of the proximal part of styloid process while distal part was still present (Figures 18A-F). I also analyzed effects of ectopic expression of *dHand*, which is one of the main downstream effectors of Edn1-Dlx5/6 and necessary for development of the most ventral part of PAs [4,31,59-61]. In *Ednra*$^{dHand/+}$ chimeric mice, in which the maxillary bone was transformed into the dentary [4], only proximal part of the styloid process was absent in the similar manner with *Ednra*$^{Edn1/+}$ mice (Figures 18G-I). These results indicate ectopic Edn1-Dlx5/6 cascade is detrimental for proper development of the proximal part of the

styloid process, suggesting that this component is generated from Edn1-Dlx5/6-negative CNCCs. Indeed, consistently with this view, defect of the styloid process in *Dlx1/2*-null mice seems limited to only the proximal part (Figures 18J, K) [53], indicating that the proximal part of the styloid process is specified by only *Dlx1/2*, while the distal part is determined by Edn1-Dlx5/6 cascade.

During developmental process, the styloid process has been described to be derived from two cartilaginous nodules, the laterohyal (tympanohyal) and stylohyal. The laterohyal joins to the otic capsule, and stylohyal fuses to the ventral laterohyal, resulting in the prominent styloid process [47]. Taken together with my observation, the laterohyal and stylohyal should correspond to the proximal and distal parts of the styloid process, respectively (Figures 20F, 21).

The distal part of the styloid process is the serial homologue of the Meckel's cartilage

On the premise that all the gnathostomes share the common blue-print of the "*Dlx*-code" [51,56,57], my developmental analysis should be useful to infer the evolutionary origin of the styloid process. In elasmobranchs and teleosts, the dorsal part of hyomandibular is generated from *Edn1-Dlx5/6*-negative region [51,58]. Based on this,

the proximal part of styloid process should have the homology with the hyomandibular of elasmobranchs (Figure 19A).

As for the distal part of styloid process, because the ceratohyal and the ventral region of the hyomadibula are developed from *Edn1-Dlx5/6*-negative region in elasmobranchs and teleosts [51,58], it should be essential to dissect whether this part corresponds to the hyomandibular or to the ceratohyal of elasmobranchs (Figure 19A).

To dissect the evolutionary origin of the distal part of the styloid process, I analyzed the PA1-derived ectopic styloid process of NCC-*Hoxa2* mice. In these mice, the malleus and the proximal part of Meckel's cartilage became absent, and instead, the ectopic styloid process was generated in their positions (Figures 19B-I). As described above, the distal part of the Meckel's cartilage was not absent in NCC-*Hoxa2* mice (Figure 3), and I found that the ectopic styloid process was almost attached to the remaining Meckel's cartilage (Figures 19H, I). These results indicate that the malleus and Meckel's cartilage transformed into the distal part of styloid process in NCC-*Hoxa2* mice, and that they are the serial homologue of the distal part of the styloid process. Previous studies have shown that the mammalian malleus is evolutionary derived from the proximal articular region of Meckel's cartilage of elasmobranchs and teleosts [47], and the Meckel's cartilage has been proved to be the serial homologue of the ceratohyal

in zebrafishes [37,41,62], therefore these results indicates that the distal part of mammalian styloid process should be evolutionary homologue of the elasmobranch ceratohyal.

Differential functional property between the distal and proximal part of the styloid process

I then dissected the mechanical functional difference between the proximal and distal styloid process by three-dimensional reconstructions of the musculature. In wild-type mice, the styloid process works as origins of muscles including the stylohyoid, stylopharyngeal and styloglossal muscles (Figure 20C). In *Ednra*-null mice, in which the distal part of the styloid process is absent, such muscles were not attached to the styloid process (Figure 20D), and instead in some cases, the stylohyoid and stylopharyngeal muscles had attachment to an abnormally condensed cartilage around the middle ear (Figures 20B, D). On the other hand, in $Ednra^{Edn1/+}$ mice, although they do not had the proximal part of the styloid process, muscle attachment to the styloid process was not affected (Figure 21E). These results indicate that the distal ceratohyal-derived component of the styloid process works as a muscle adhesion

scaffold, while the proximal hyomandibular-derived component works as an anchor structure which connects the distal styloid process and otic capsule.

Discussion

Having three middle ear ossicles is a fundamental morphological feature of mammals, and this issue has attracted considerable attention of comparative zoologists for about 200 years [45,46]. To understand apparently different middle ear morphology among amniotes, identification of precise homology between PAs-derived structures should be essential. In this chapter, I re-examined the evolutionary and developmental origins of the styloid process, a mammalian-specific PA2-derived structure, and revealed that the styloid process is evolutionary derived not only from the hyomandibular but also from ceratohyal components, and identified that dorsoventral (hyomandibular/ceratohyal) boundary of PA2 exists in the middle of styloid process.

This finding can bring about re-interpretation about the evolutionary process of the middle ear in vertebrates. Recent paleontological observation has revealed that ancestral synapsids did not possess the functional middle ear, and the modern consensus is that the middle ear of mammals and diapsids developed independently after their divergence from a common ancestral amniote [63-67]. In diapsids, connectivity between the hyomandibular and palatoquadrate was cancelled, and the hyomandibular was utilized as a single middle ear ossicle which connects the tympanic membrane and fenestra ovale. On the other hand, in synapsids, in addition to the hyomandibular, the

primary jaw joint was also introduced into the sound transmitting system, resulting in three middle ear ossicles, and the dorsal process of the hyomandibular was separated from the main unit and inserted into the otic capsule to form the mammalian styloid process. My observation reveals more detailed evolutionary process of reorganization of mammalian PA2-derived skeletons. During the mammal-specific middle ear evolution, in addition to evolutionary events described above, fusion between the ceratohyal (stylohyal) and hyomandibular (laterohyal) components should have occurred. Furthermore, the laterohyal should have separated from the main body of the ceratohyal, and the laterohyal and hyoid bone, which should be evolved from the main body of the ceratohyal, were connected by the stylohyal ligament (Figure 21). To understand proper sequence of these events, future paleontological observation should be essential.

Although homology of the middle ear and jaw skeletons between mammals and amniotes has been well studied, developmental or molecular mechanism which allowed them to evolve such evolutionary distinct middle ear systems is hitherto not disclosed. Recently, Takechi et al suggested that the tympanic membrane may be non-homologous structures and can be a key to solve this issue [45]. The tympanic membrane of diapsids is apparently attached to the quadrate, the upper jaw element, while that of mammals spans the ectotympanic, the angular homologue belonging to the lower jaw. Therefore,

dissecting dorsoventral patterning of PAs among amniotes can be prospective approach, and this study can provide a properly organized framework to understand development of the mammalian middle ear.

The proximal and distal parts of the styloid process have division of work: the stylohyal works as a muscle adhesion scaffold, while the laterohyal works as a mediation of the stylohyal and otic capsule. Indeed, the distal styloid process functionally resembles the hyoid bone to which several suprahyoid and inferahyoid muscles are also connected. On the assumption that the ceratohyal was separated into two parts and evolved the mammalian laterohyal (distal styloid process) and hyoid bone, it may be reasonable to regard this set as the "hyoid bone" from an evolutionary perspective (Figure 20F). Indeed, some comparative anatomical observations have also indicated that the mammalian hyoglossal and styloglossal muscles correspond to dipasids or amphibian hyoglassal muscle [68,69]. From an adaptive perspective, ancestral synapsids were selected to masticate substance for a longer time, and consequently the dentary bone grew larger and the secondary jaw joint evolved [70]. The secondary palate was also adaptive because it allowed breathing during mastication. In this context, complex tongue and pharyngeal movement might also be effective for longer mastication, and as a result the dorsal part of the ancestral "hyoid bone"

(stylohyal) might be separated from the main body and fixed to the otic capsule via the laterohyal to achieve advanced tongue and pharyngeal movement. As for induction of the hyomandibular into the styloid process, hyomandibylar loss of function as a jaw anchorage device might be critical. In ancestral vertebrates, the upper jaw was fixed to the neurocranium via the hyomandibular, but in ancestral amniotes the enlarged paroccipital process of opisthotic bone became to fix the upper jaw to the neurocranium, and consequently the hyomandibular was allowed to evolve sound transmitting devices such as the stapes and columella auris [66], and moreover, the dorsal process of hyomandibular might have a chance to be separated from the main body to generate the proximal part of the styloid process to support tongue and pharyngeal movement. Because appearance of the secondary jaw joint, consequent reduction of the primary jaw joint and loss of hyomandibular function as an anchor device has been indicated to have a close relation with evolution of middle ossicles [66,70], my insights may provide a novel framework to understand evolution of vertebrate PAs, integrating evolution of the styloid process, hyoid apparatus and middle ear system of mammals.

Part 3:

Independent origins of tympanic membranes and middle ears in amniotes

Summary

Evolution of the mammalian middle ear has long been a formidable conundrum of vertebrate morphology. Since steadfast morphological homologies of skeletal elements have been formulated in amniote middle ears, difficulties remain in recognizing truly novel patterns tied to the evolutionary changes in developmental programs both in diapsids and mammals. Here I show, through developmental experiments, that independent origins of the tympanic membranes had brought about the middle ear structures in different manners in the amniote evolution. By inactivation of Endothelin1-Dlx5/6 cascade, a switch that specifies ventral identity of pharyngeal arches, the tympanic membrane was absent in the mouse, whereas it was duplicated in the chicken. These results indicate that the tympanic membrane is developmentally coupled with the lower jaw in mammals, while that of diapsids with the upper jaw. Consistently, I reveal that the topographical relationships between the first pharyngeal pouch and the primary jaw joint distinctly differ between the two animals - the joints are formed dorsal to the pouch in mouse, and ventral to the pouch in the chicken embryos. A genetic cascade involving *Goosecoid* is always associated with the lower jaw, but is indispensable for tympanic membrane development only in mammals. I conclude that this different relative positioning of primary jaw joint and the first pharyngeal pouch lead to two distinct middle

ears of amniotes, with different number of ear ossicles.

Introduction

The sense of hearing is an important adaptive trait for animals in hunting, escaping, courting, and other social behaviors, and amniotes possess highly sophisticated impedance-matching auditory system, in which the air vibration received by the tympanic membrane with comparatively large surface area and low acoustic-impedance is transferred by the middle ear to the inner ear [71]. Based on the fossil record, the amniote middle ear appears to have evolved polyphyletically [63,72], and that in crown synapsids (modern mammals) stands out conspicuously in the possession of three middle ear ossicles, as compared to that in diapsids where only one ossicle, columella auris (= stapes), that arises from the second pharyngeal arch (PA2). It has long been shown that the excessive two ossicles in mammals, malleus and incus, are homologous with articular and quadrate, primary jaw joint (PJJ) elements [45,73]. From the perspective of evolutionary developmental biology, therefore, different patterns of middle ears should be ascribed to changes in developmental program for PA1 and PA2 [45].

One of the difficulties associated with the middle ear is that morphological homology has been established for every skeletal and muscular element between mammals and

diapsids, making it intricate to qualify the novelty of either mammalian or diapsid middle ear [73-75]. Curiously, however, a significant difference has been recognized in the relative position of the tympanic membranes (TMs) between mammals and diapsids [45,73]. In diapsids, TM attaches to the quadrate, an upper jaw element, while in mammals, TM spans the ectotympanic, the angular homologue belonging to the lower jaw (Figure 22A).

Results

Assuming that the TM formation is coupled with patterning either of upper and lower jaw, experimental transformation between the upper and lower jaws should affect development of the TM in different ways in each animal lineage. To exemplify this, experimental intervention into *Endothelin1* (*Edn1*) signaling in pharyngeal arches (PAs) would serve as a prospective approach: *Edn1* signaling regulates *Dlx5/6* in ventral region of PAs, whereby specifying the lower jaw and the primary jaw joint (PJJ; the articulation in the quadrate and articular homologues) through establishing the *Dlx*-code in PAs [22,31,52]. Indeed, inactivation of *Edn1* and its receptor, *Endothelin receptor type A* (*Ednra*), results in the loss of the lower jaw identity and transformation of the lower jaw into upper jaw in mirror image as in the case of the *Dlx5/6*-null mouse [2,3,31-33]. Therefore, we first observed the skeletal morphology and TM in the *Ednra*-null mouse (Figures 22B-E).

In the middle ear of the *Ednra*-null mouse, invagination of the external auditory canal were missing together with the TM (Figures 22D, E; compare with Figures 22B, C). These results indicated that development of the TM depends on that of the lower jaw in the mouse, consistent with the recent report that the external auditory

canal does not correspond to the first pharyngeal cleft (between PA1 and PA2), but emerges within PA1 [54].

We then performed equivalent inhibition of Edn1-Dlx5/6 cascade in the chicken using bosentan, an Edn receptor antagonist. As in the mouse, bosentan treatment resulted in down-regulation of *Dlx5/6* (Figures 23A-D) and transformation of the lower jaw morphology into the identity of the upper jaw (Figures 23E-I). Unlike in the mouse, however, a supernumerary external auditory canal appeared ventral to the original one (Figures 22F, K), resulting in a mirror-image duplicated TMs (Figures 22G-I, L-O). Thus, equivalent developmental perturbations induced identical phenotypes in the patterning of jaw skeletons, but different phenotypes were obtained for the development of TMs between mouse and chicken embryos (Figure 22P).

To understand why the inhibition of the Edn1-Dlx5/6 cascade induced the opposite phenotypes of TMs in the mouse and chicken, we investigated gene expression pattern involved in the jaw and middle ear patterning in both animals. *Goosecoid* (*Gsc*) is one of downstream targets of the Edn1-Dlx5/6 cascade [76]. Its inactivation in mice results in hypoplasia of external auditory canal and the ectotympanic (homologue of the angular in non-mammals)[77], suggesting that external auditory canal is induced as a lower jaw component. Indeed, *Gsc* expression was associated with the TM and

ectotympanic primordia in the mouse (Figures 24A, B). In contrast, the chicken *Gsc* was also detected in the angular, but not around the TM that is found more dorsally (Figures 24C, D). These results suggested that *Gsc* is commonly involved in the proximal part of the ventral PA1, and only in the mouse, it is involved in the TM patterning. Although the TM of mammals and diapsids are functionally comparable, they are coupled with different components of PA1 (Figure 22P).

The different roles of *Gsc* in mouse and chicken embryos appear to reflect difference in relative topographical relationships between the TM (reflecting the position of the first pharyngeal pouch, PP1) and the PJJ in the mouse and chicken. In embryos of both the animals, PP1 forms by the same manner in a same relative position between PA1 and PA2 (Figure 25). We then examined expression of *Bapx1*, a marker gene for the PJJ mesenchyme [78], and found that it was expressed more dorsally in the mouse as compared to the chicken, in proximity to PP1 (Figures 26A-D). This difference became more enhanced in development, to result in the formation of the procartilaginous PJJ adjacent to PP1 in the mouse, and ventral to PP1 in the chicken (Figures 26E, F): the external auditory canal invaginates ventral to the PJJ in the mouse, and dorsal to the PJJ in the chicken (Figures 26E, F). It is therefore the relative positions of skeletal and TM components that differ between the two animals.

Discussion

Our results are highly relevant to the differential patterns of the middle ears between mammals and diapsids. To explain the inconsistent position of TMs between mammals and diapsids, conventional hypotheses assumed either a ventrad shift of ancestral TM [47,79] or a *de novo* acquisition of TM associating with an imaginary ventrad swelling of the middle ear cavity [80] in mammals. The latter hypothesis, however, is not consistent with the mammalian-specific distribution of neural crest cells-derived epithelium in the middle ear cavity [81]. We showed that both the TMs differentiate from a comparable embryonic anlage (PP1), and PP1 is developmentally equivalent in mouse and chicken, and there was no secondary ventral swelling of PP1 in the mouse (Figures 26E, G). Most importantly, PJJ primordia develop in relatively different positions with respect to PP1 between avian and mammalian embryos (Figure 26). The most plausible explanation would simply be that a topographical frameshift between PP1 and the PJJ established different middle ears between mammalians and diapsids.

Assuming that the TM was acquired independently in synapsids and diapsids, our observation suggested that these two lineages have undergone topographically different modification to obtain similar auditory functions. During this evolution, the

molecular mechanism to specify PA skeletal elements through the Edn1-Dlx5/6 cascade is rather rigidly conserved in mammals and diapsids. Indeed, the equivalent inhibition of the cascade resulted in identical phenotypes with respect to the skeletal identities between the mouse and chicken (Figure 22). Even in chondrichthyan embryos, an equivalent *Dlx*-code is established [51]. Given that *Bapx1* and *Gsc* are expressed in a homologous set of skeletal elements in the mouse and chicken (Figures 24, 26), the whole gene expression patterns in the PAs can be regarded as a highly conserved interactive gene regulatory network that assures the morphological homologies of PA skeletal elements in gnathostomes. This, however, does not appear to involve TM development automatically. The TM forms through interactions among PP1, external auditory canal and surrounding mesemchyme [82], which are also conserved between mouse and chicken (Figures 25, 26). Collectively, it can be rationalized that the developmental program for skeletal specification and that for TM are primarily decoupled from each other, and secondarily the latter was coupled with the upper and lower PA1 components in the chicken and mouse, respectively, to obtain topographically distinct TMs independently.

According to paleontological evidence of the outgroup, the quadrate, articular and hyomandibular in basal amniotes were more robust than modern amniotes

[63,83-85], suggesting that the positional interrelationship between PP1 and PJJ in basal amniotes was likely similar to that seen in crown diapsids (Figure 27A). Stem synapsids and stem diapsids had still retained the plesiomorphic (or chondrichthyan-like) jaw suspension using the hyomandibular articulated with the quadrate, which, later became relaxed due to the newly established bony connection between the paroccipital process of the opisthotic and the skull roof in the diapsid lineage, and finally the quadrate-hyomandibular articulation is canceled [66]. In the synapsid lineage, on the other hand, the original articulation among the hyomandibular, quadrate and articular had always been retained, disabling the possession of hyomandibular-associated TM [73,74]. As shown above, the mammalian-specific dorsal shift of PJJ position with respect to the PP1 is apomorphic for crown synapsids. This shift would then have permitted the formarion of the unique lower jaw-associated TM in mammals. It is thus conceivable that the difference in the connection and release among these skeletal elements likely played a role of key innovation, marking the watershed of subsequent evolution of two distinct middle ear in amniote evolution (Figures 27B, C). Our findings in developmental aspect, along with future analyses in functional aspects of the PA derivatives, will permit us to fully understand the driving forces in evolution of the amniote middle ears.[74][80,86,87][81]

[76][47,79]

General Discussion

PAs of vertebrates are characteristic metameric structures, and elaborated craniofacial structures are generated by their metamorphoses. In PAs, there exists intricate interaction between various tissues such as CNCCs, endoderm, ectoderm, mesoderm, neural epithelium and so on. Craniofacial components are among the most variable structures in vertebrates, and evolution of the mammalian middle ear has especially attracted considerable attention of comparative zoologists for more than 200 years. Recent progress of experimental developmental biology and molecular biology has revealed that several gene families are important for regionalization of PAs: *Hox* and *Dlx* genes specify PAs along anteroposterior and dorsoventral axes, respectively.

Here I dissected the property of the *Hox*- and *Dlx*-codes of PAs, and tackled on the evolution of the mammalian middle ear by experimental approach. I found that expression of *Hox* genes in CNCCs is essential and sufficient for regionalization of PAs. Furthermore, I utilized several *Hox* and *Dlx* genes related mutant mice, and identified the dorsoventral (hyomandibylar/ceratohyal) boundary of mammalian PA2. Furthermore, I also revealed independent origins of tympanic membranes and middle ears by intervention on Edn1/Dlx5/6 cascade in the mouse and chicken: the mammalian

tympanic membrane is coupled with the lower jaw development, while the tympanic membrane of diapsids is coupled with the upper jaw. Topographical change between the PJJ and PP1 was critical for this difference.

Previously, paleontological observation has mainly provided major knowledge on the evolution of the middle ear among amniotes, but here my experimental developmental approach could provide a new perspective on this issue. Future analysis of PA regionalization should be essential to better understand evolution and development of vertebrate craniofacial structures, and in this context, integration of anteroposterior and dorsoventral axes by dissecting possible crosstalk between the *Hox*- and *Dlx*- code can be a prospective novel approach.

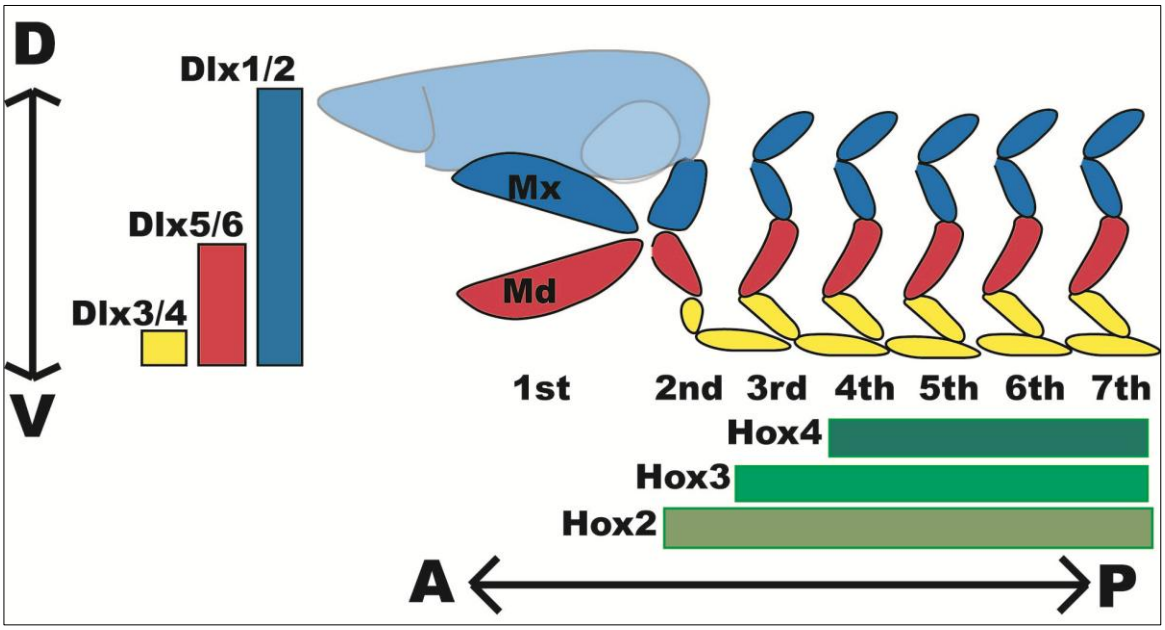

Figure 1. The basic pattern of the *Hox*-code and the *Dlx*-code in pharyngeal arches (PAs) of vertebrate. After Depew et al. (2002).

Hox genes specify anterior-posterior identity and *Dlx* genes specify dorsal-ventral identity of PAs. 1st - 6th, 1st -6th pharyngeal arches; Md, mandibular process; Mx, maxillary process.

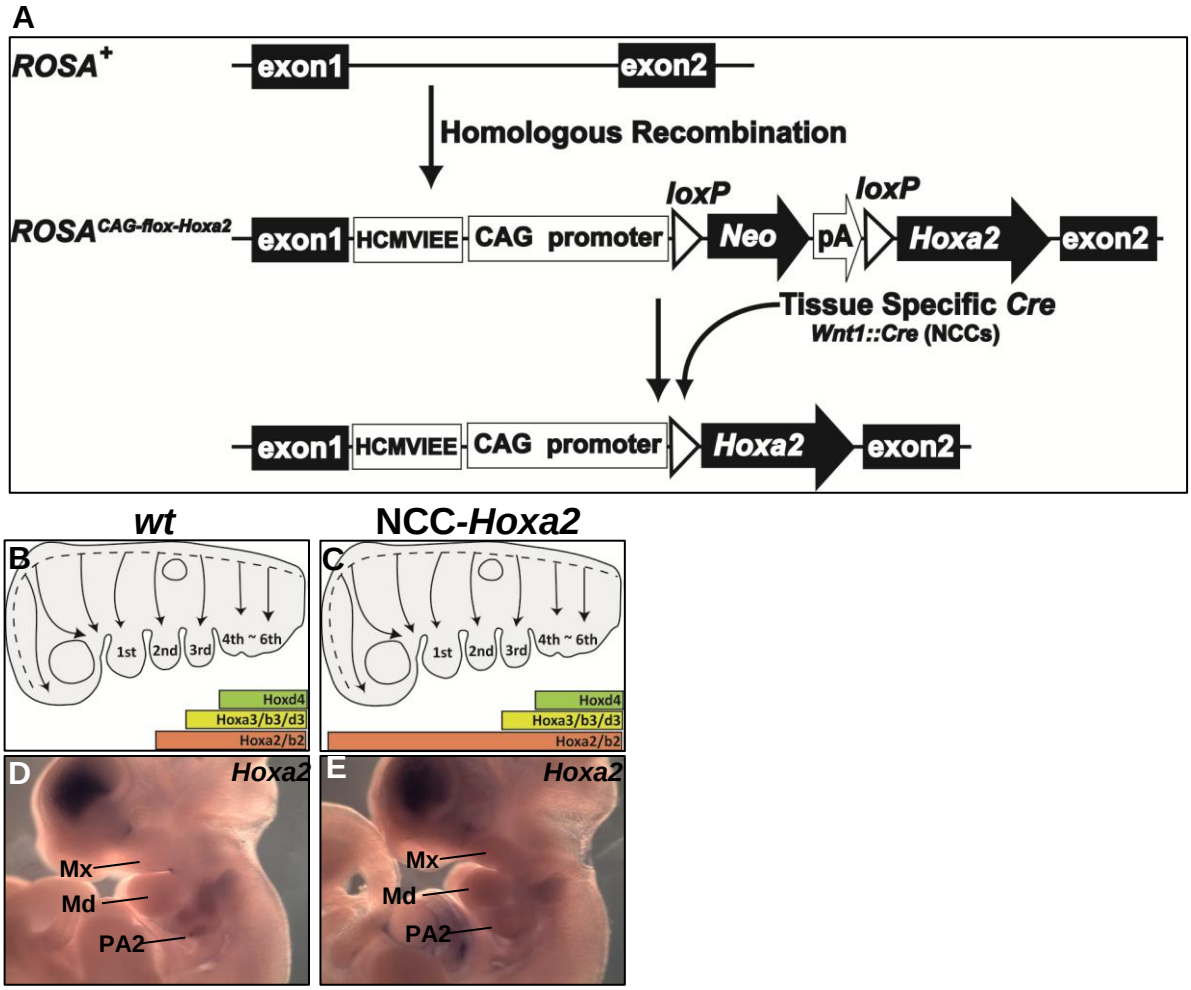

Figure 2. CNCCs-specific over-expression of *Hoxa2*

(A) A schematic representation of conditional over-expression of *Hoxa2* driven by CAG promoter. A cassette of HCMVIEE, CAG promoter, *loxP*-STOP (*Neo*-pA)-*loxP* and *Hoxa2* is knocked-in between *ROSA26* locus (ROSA$^{CAG\text{-}flox\text{-}Hoxa2}$). *Wnt1::Cre* induce NCC-specific over-expression (NCC-*Hoxa2*). (B, C) Summary of knock-in mice. In wild-type, neural crest cells (NCCs) which migrate to the PA1 and more anterior region are *Hox*-negative (B). To achieve ectopic expression of *Hoxa2* in NCCs, conditional over-expression of *Hoxa2* is driven downstream of CAG promoter by *Wnt1::Cre* (NCC-*Hoxa2*) (C). (D,E) Whole mount in situ hybridization of E10.5 wild-type (D) and NCC-*Hoxa2* (E). 1st -6th, 1st -6th pharyngeal arches; CAG promoter, *chicken bera-actin* promoter; HCMVIEE, human cytomegalovirus immediate-early enhancer; Md, mandibular process; Mx, maxillary process; *Neo*, neomycin; pA, poly A sequence; PA1, 1st pharyngeal arch; PA2: 2nd pharyngeal arch; *Puro*, puromycin.

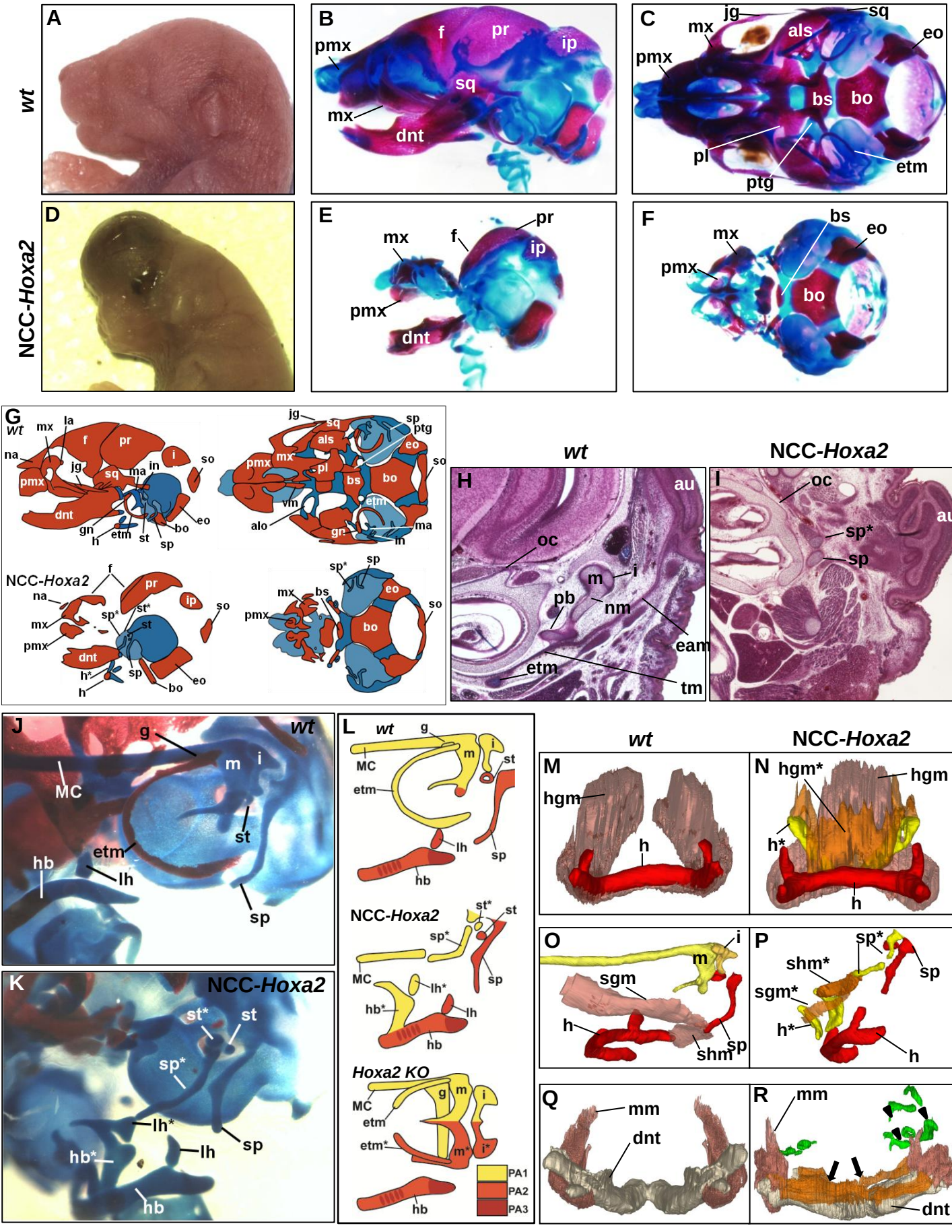
wt
NCC-Hoxa2
A
B
C
D
E
F
pmx
f
pr
ip
sq
mx
dnt
jg
als
eo
bs
bo
pl
ptg
etm
G
wt
la
na
jg
ma
in
so
gn
h
sp
ptg
vm
alo
gr
NCC-Hoxa2
sp*
st*
st
H
I
au
oc
m
i
pb
nm
eam
tm
J
g
MC
hb
lh
K
st*
sp*
lh*
hb*
L
Hoxa2 KO
PA1
PA2
PA3
M
N
hgm
hgm*
h
h*
O
P
sgm
shm
shm*
sgm*
Q
R
mm
dnt

Figure 3. NCCs-selective ectopic expression of *Hoxa2* is sufficient for homeotic transformation from the PA1 to PA2.
(A, D) Lateral appearance of E17.5 wild-type (A) and NCC-*Hoxa2* (D) mice. (B, E) Lateral views of E17.5 wild-type (B), and NCC-*Hoxa2* (E) cranial skeletal structures. (C, F) Ventral views of E17.5 wild-type (C), and NCC-*Hoxa2* (F) cranial skeletal structures. (G) A schematic representation of lateral and ventral views. (H, I) Frontal sections of E17.5 wild-type (H) and NCC-*Hoxa2* (I) mice. (J, K) lateral-ventral views of skeletal structures around the middle ear of E17.5 wild-type (J) and NCC-*Hoxa2* (K) mice. The dentary is removed. (L) A schematic representation of homeotic transformation of PAs induced by misexpression of *Hoxa2*. (M-N) Three-dimensional reconstruction of E17.5 wild-type (M, O, Q) and NCC-*Hoxa2* (N, P, R) mice. Dorsal views of the hyoid bone (M, N), lateral views of the left side around the middle ear, (O, P), and dorsal views of the dentary (Q, R). Black arrowheads indicate ectopic cartilages in the cranial base, and black arrow indicates ectopic muscle which connects the geniapophysis and angular process of the dentary (R). als, alisphenoid bone; bo, basioccipital bone; bs, basisphenoid bone; dnt, dentary; eam, external acoustic meatus; eo, extraoccipital bone; etm, ectotympanic process; f, frontal bone; gn, gonial bone; h, hyoid bone; hb, hyoid body; hgm, hyoglossal muscle; lh, lesser horn; i, incus; ip, interparietal bone; jg, jugal bone; la, lacrimal bone; m, malleus; MC, Meckel's cartilage; mm, musculation muscle; mx, maxilla; na, nasal bone; nm, neck of malleus; oc, otic capsule; pb, processus brevis of malleus; pl, palatine bone; pmx, premaxilla; pr, parietal bone; ps, preshenoid bone; ptg, pterygoid bone; sgm, styloglossal muscle; shm, stylohyoid muscle; so, supraoccipital bone; sp, styloid process; sq, squamous bone; st, stapes; tm, tympanic membrane; *, duplicated structure.

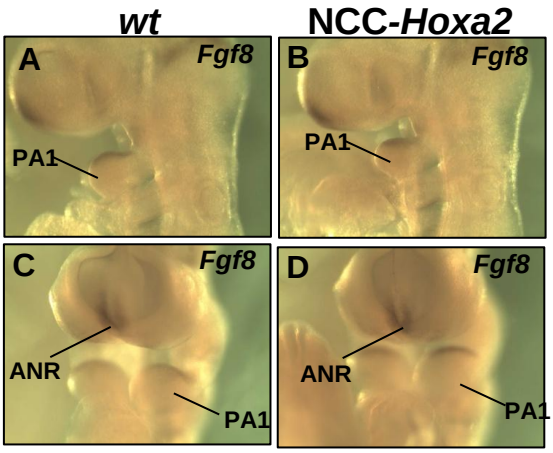

Figure 4. Expression of *FGF8* is not disturbed by ectopic expression of Hoxa2 in CNCCs. (A-D) Whole mount in situ hybridization of E9.5 wild-type (A, C) and NCC-*Hoxa2* (B, D) mice for *Fgf8*. ANR, anterior neural ridge; PA1, 1st pharyngeal arch.

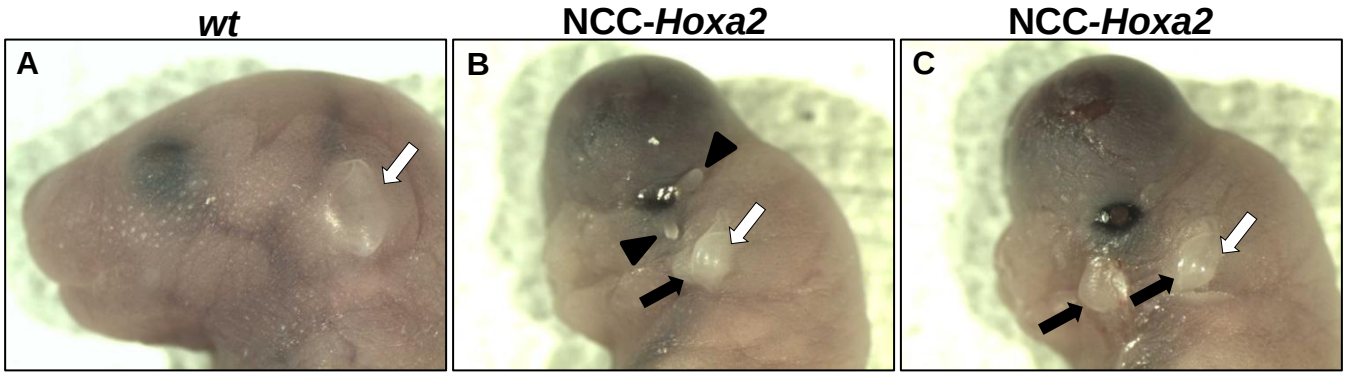

Figure 5. CNCCs-specific over-expression of *Hoxa2* induce homeotic transformation of the auricle.

(A-C) Facial appearance of E18.5 wild-type (wt) (A) and NCC-*Hoxa2* (B, C) mice. White arrows indicate original auricles derived from the PA2, black arrows indicate ectopic auricles derived from the PA1, and black arrow heads indicate small auricle-like processes.

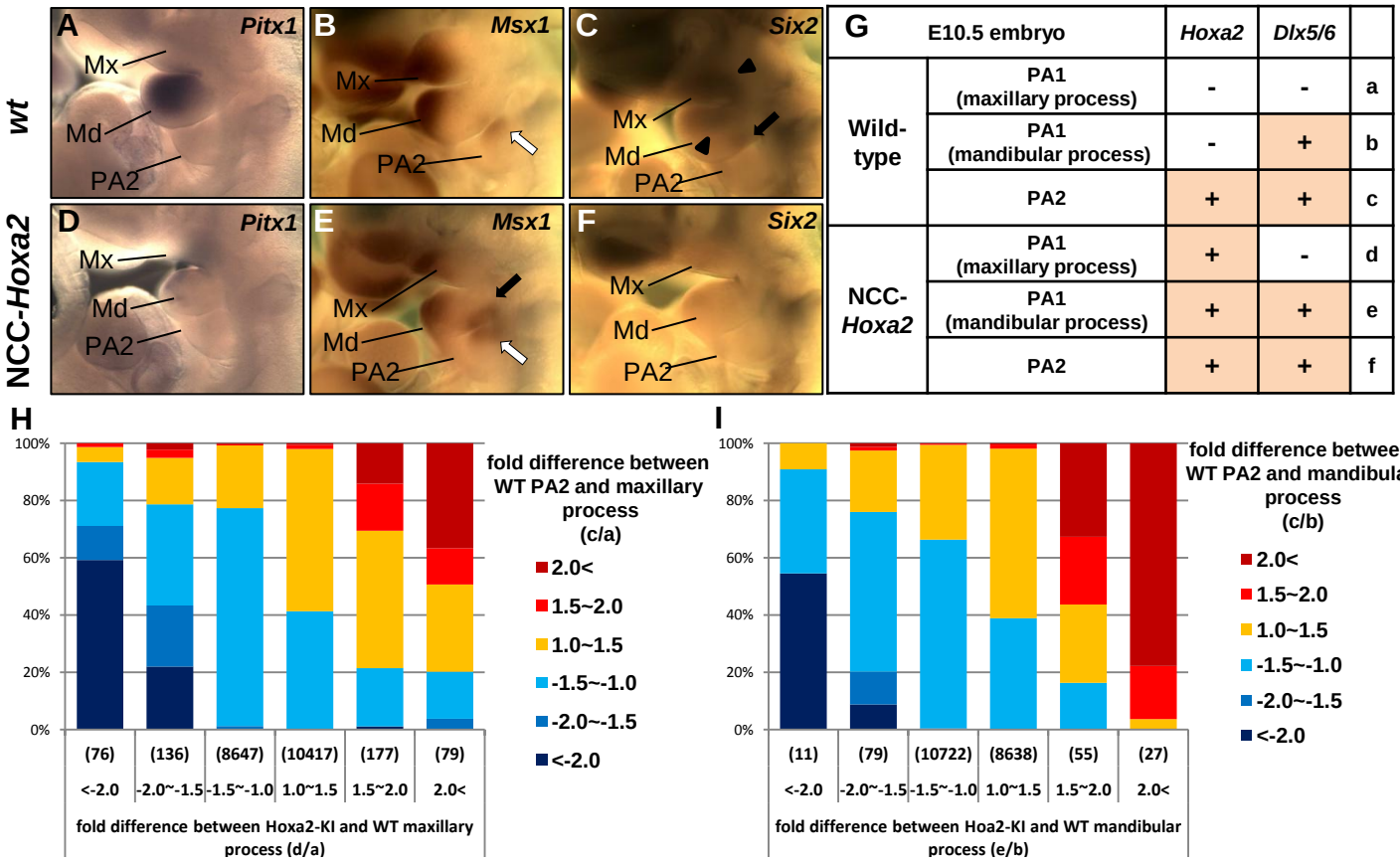

Figure 6. NCCs-selective ectopic expression of *Hoxa2* re-patterns gene expression of the PA1.
(A-F) Whole mount in situ hybridization of E10.5 wild-type (A-C) and NCC-*Hoxa2* (D-F) for *Pitx1* (A, D), *Msx1* (B, E) and *Six2* (C, F). Expression of *Msx1* in the PA2 is indicated by a white arrow, and duplicated expression in the PA1 is indicated by a black arrow (B, E). Expression of *Six2* around hinge region of the PA1 is indicated by black arrow heads, and expression in caudal region of the mandibular process is indicated by black arrow heads (C).
(G) A list of six transcriptome samples of PAs from E10.5 wild-type and NCC-*Hoxa2* mice. Corresponding *Hoxa2* and *Dlx5/6* expression patterns and alphabetical symbols are also indicated. (H, I) Fractional analysis demonstrating changes of transcriptional profile of PA1 into PA2. (H) shows changes of maxillary process; in a horizontal axis, about 20,000 genes are divided into six fractions according to fold difference between the maxillary process of NCC-*Hoxa2* and wild-type mice (d/a). Number of genes in each fraction is indicated in parentheses. Next, each fraction is further divided into six subfractions according to fold difference between the PA2 and the maxillary process of wild-type mice (c/a). (I) shows changes of the mandibular process in the same manner with the maxillary process.
Md, mandibular process; Mx, maxillary process; PA, pharyngeal arch.

A

	E10.5 embryo	*Hoxa2*	*Dlx5/6*	
Wild-type	PA1 (maxillary process)	-	-	a
	PA1 (mandibular process)	-	+	b
	PA2	+	+	c
NCC-*Hoxa2*	PA1 (maxillary process)	+	-	d
	PA1 (mandibular process)	+	+	e
	PA2	+	+	f

B *wt* vs NCC-*Hoxa2*-PAs — 178 genes

Category	Count	%	FDR
transcription factor activity	38	22.1	1.38E-15
Homeobox	22	12.8	3.15E-12
embryonic morphogenesis	22	12.8	2.64E-08
pattern specification process	17	9.9	1.44E-05
neural crest cell development	6	3.5	0.0206313

C

		NCC-*Hoxa2* vs wt maxillary process (d/a) this study,	
		UP	DOWN
Hoxa2 KO vs wt PA2 Donaldson et al. (2012)[2]	UP	1	20
	DOWN	49	9

D

		NCC-*Hoxa2* vs wt mandibular process (e/b) this study	
		UP	DOWN
Hoxa2 KO vs wt PA2 Donaldson et al. (2012)[2]	UP	0	9
	DOWN	23	2

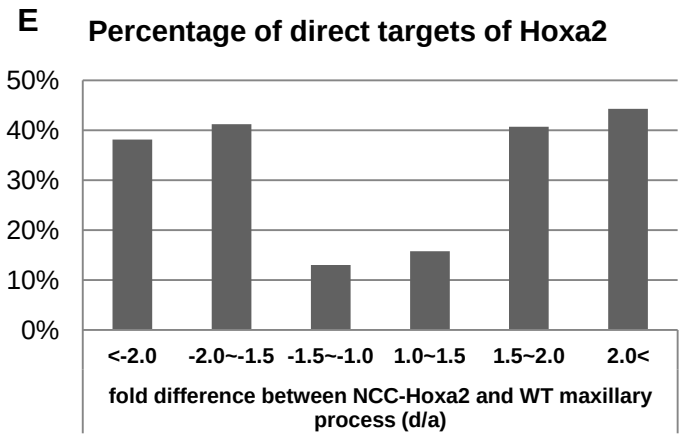

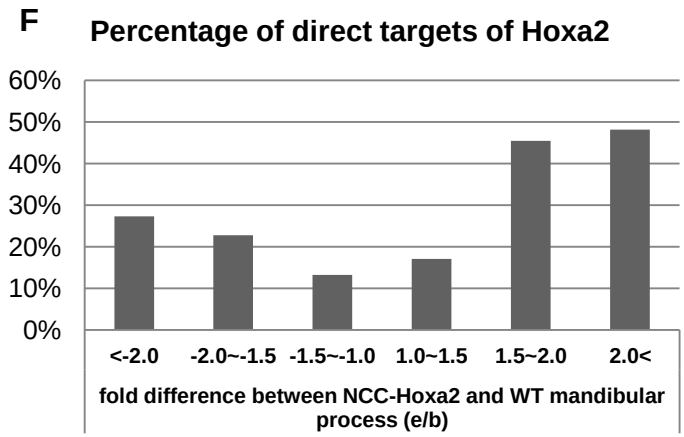

Figure 7. Ectopic *Hoxa2* induce transformation of gene expression pattern.
(A) A list of six transcriptome samples of PAs from E10.5 wild-type and NCC-*Hoxa2* mice. Corresponding *Hoxa2* and *Dlx5/6* expression patterns and alphabetical symbols are also indicated. (B) Gene ontology analysis of transcriptome. Out of about 20,000 genes examined, genes which showed up- or down-regulation more than 2 folds are picked up by comparison between wild-type and NCC-*Hoxa2* mice (178 genes), and these genes are analyzed for ontology. (C, D) Comparison of gene expression profiles between *Hoxa2* knock-in (NCC-*Hoxa2*) and *Hoxa2* knock-out mice. Previous study showed a list of direct targets of *Hoxa2* in the PA2 that are considerably up- or down-regulated in *Hoxa2*$^{-/-}$ mice (Donaldson et al. (2012)). We picked up genes that are up- or down-regulated more than 1.5 folds in the maxillary process (d/a) (C) or in the mandibular process (e/b) (D) of NCC-*Hoxa2* mice respectively, and compared them with the list of Donaldson et al. (E, F) Analysis for *Hoxa2* direct target genes. We divided genes into six groups according to expression difference in the maxillary process (d/a) (E) or in the mandibular process (e/b) (F) between wild-type and NCC-*Hoxa2* mice, and calculated percentage of *Hoxa2* direct target genes within groups using ChIP-seq data from Donaldson et al.

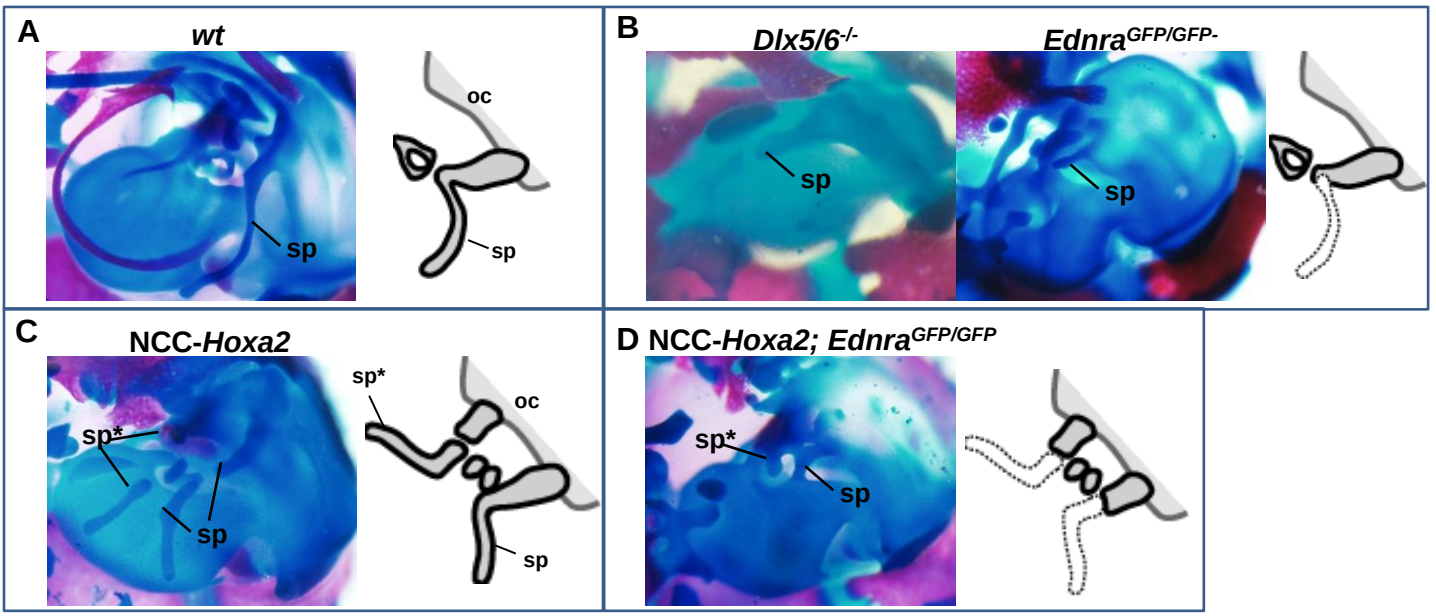

Figure 8. Properly expressed *Hoxa2* and *Dlx5/6* genes coordinately pattern the styloid process. (A-D) Skeletal structures and schematic representations of wild-type (A), *Dlx5/6*$^{-/-}$ and *Ednra*$^{GFP/GFP}$ (B), NCC-*Hoxa2* (C), and NCC-*Hoxa2; Ednra*$^{GFP/GFP}$ (D) mice.

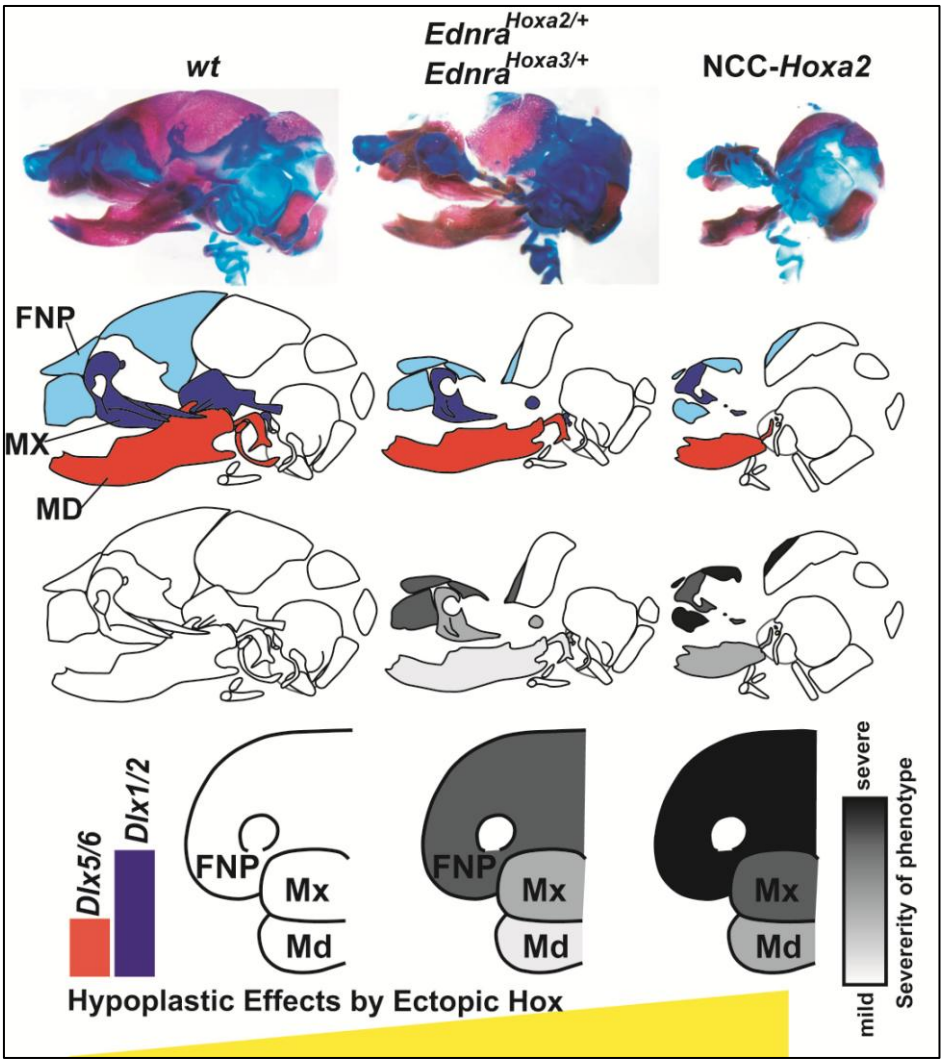

Figure 9. Hypoplasia induced by ectopic *Hox* genes correlates with expression pattern of Dlx genes. Schematic representation that ectopic *Hox* genes induce severe craniofacial phenotype in a *Dlx* genes dependant manner. FNP, frontonasal process derived structures.

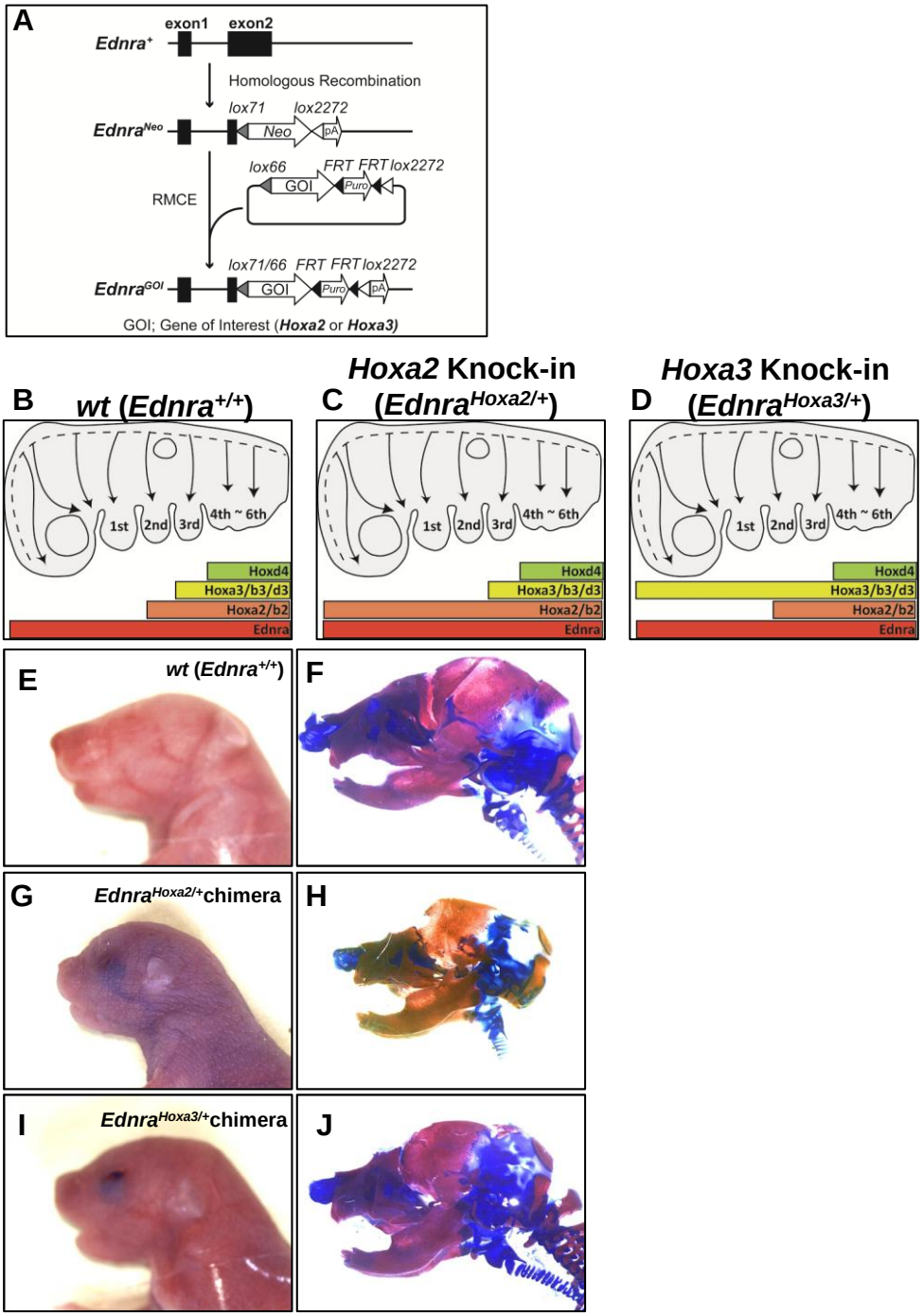

Figure 10. Over-expression of *Hox* genes by *Ednra* promoter

(A) Schematic representation of over-expression of *Hoxa2* and *Hoxa3* by RMCE (recombinase mediated cassette exchange) system in *Ednra* locus. Detailed explanation of RMCE is described in Sato et al. 2008. (B-D) Schematic representations of knock-in mice in *Ednra* locus. In wild-type, neural crest cells (NCCs) which migrate to the PA1 and more anterior region are Hox-negative, and *Ednra* is expressed in overall cranial NCCs (CNCCs) (B). *Hox* genes are knocked-in into *Ednra* locus, and ectopic expression of *Hoxa2* (C) or *Hoxa3* (D) is induced in CNCCs. (E, G, I) Facial appearance of P0 wild-type (wt) (E), $Ednra^{Hoxa2/+}$ chimera (G) and $Ednra^{Hoxa2/+}$ chimera (I) mice. (F, H, J) Lateral views of P0 wt (F), $Ednra^{Hoxa2/+}$ chimera (H) and $Ednra^{Hoxa2/+}$ chimera (J) mice cranial skeletal structures.

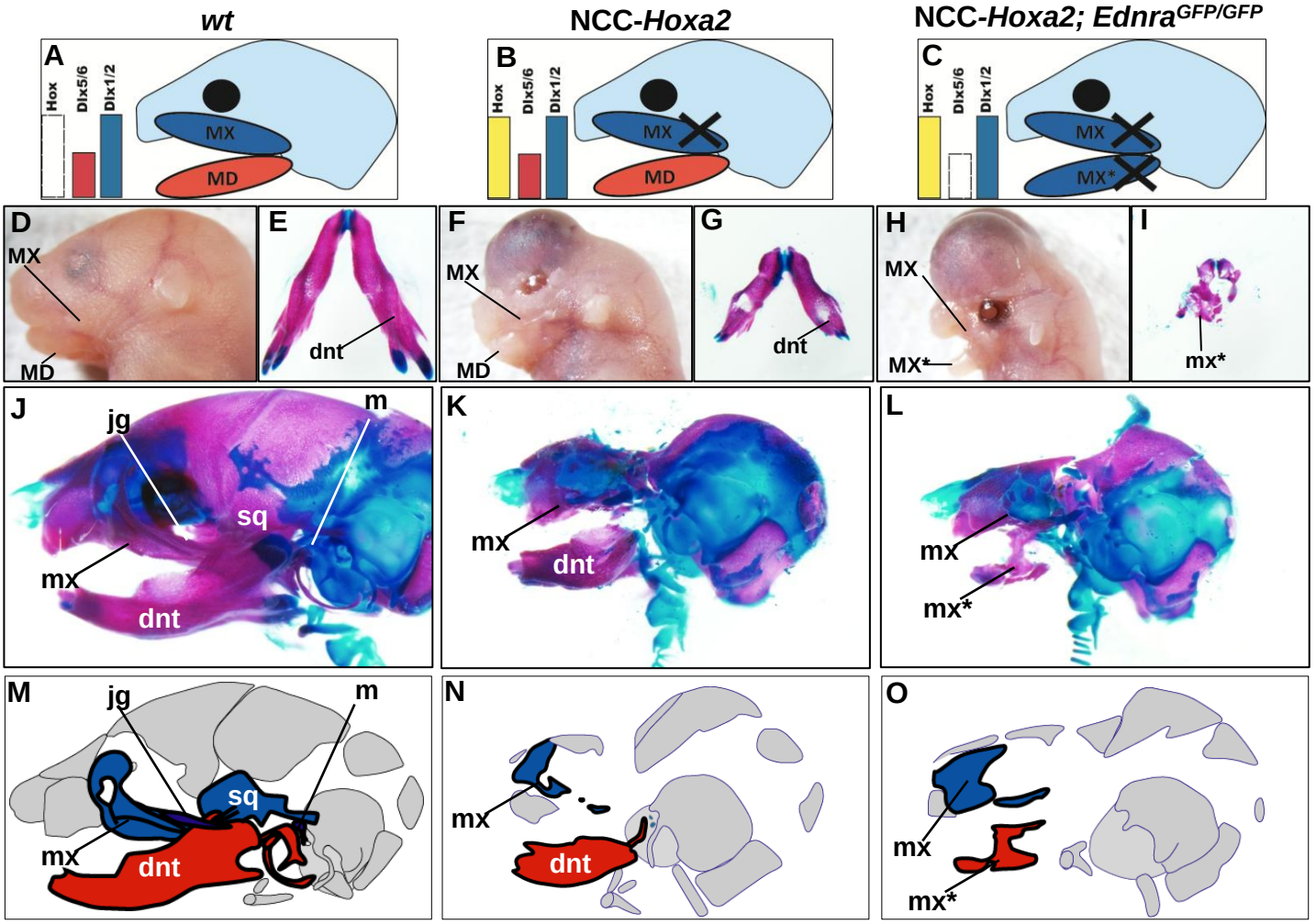

Figure 11. Ectopically induced *Hox* genes induce hypoplasia selectively in the dorsal context.
(A-C) Schematic representations of the *Hox*-code and the *Dlx*-code of wild-type (A), NCC-*Hoxa2* (B) and NCC-*Hoxa2; Ednra*$^{GFP/GFP}$ (C) mice. (D, F, H) Facial appearance of E17.5 wild-type (D), NCC-*Hoxa2* (F) and NCC-*Hoxa2; Ednra*$^{GFP/GFP}$ (H) mice. (E, G, I) Ventral views of the dentary bone of wild-type (E), NCC-*Hoxa2* (G) and NCC-*Hoxa2; Ednra*$^{GFP/GFP}$ (I) mice. (J-L) Lateral views of wild-type (J), NCC-*Hoxa2* (K) and NCC-*Hoxa2; Ednra*$^{GFP/GFP}$ (L) mice. (M-O) Schematic representations of skeletal structures of wild-type (M), NCC-*Hoxa2* (N) and NCC-*Hoxa2; Ednra*$^{GFP/GFP}$ (O) mice. Maxillary components are colored blue and mandibular ones are colored red.

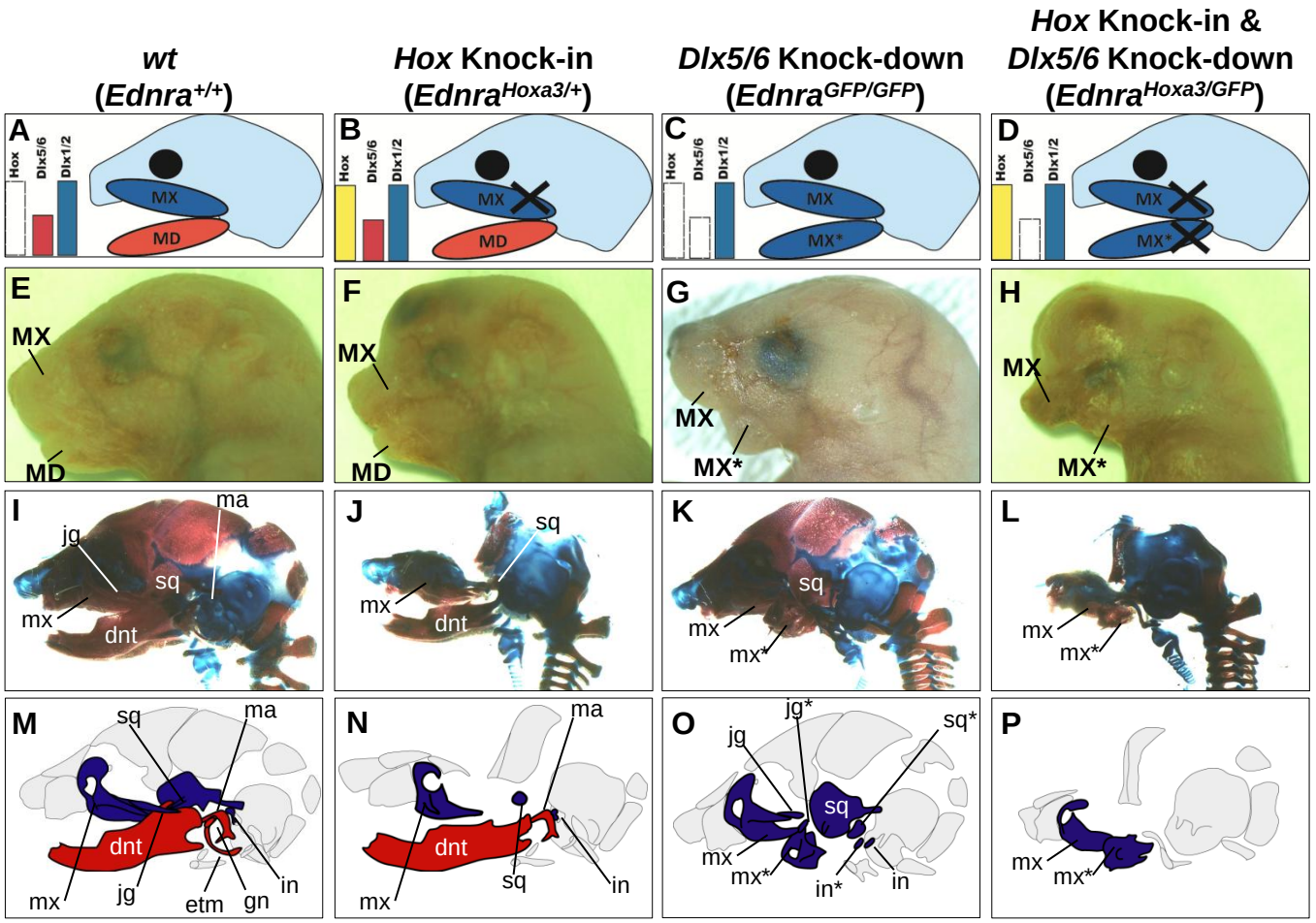

Figure 12. Hypoplasia induced by ectopic Hox genes correlates with Dlx genes expression
(A-D) Schemes of the *Hox*-code and the *Dlx*-code of wild-type (A), *Ednra*$^{Hoxa3/+}$ (B), *Ednra*$^{GFP/GFP}$ (C) and *Ednra*$^{Hoxa3/GFP}$ (D) mice. (E-H) Facial appearance of E17.5 wild-type (E), *Ednra*$^{Hoxa3/+}$ (F), *Ednra*$^{GFP/GFP}$ (G) and *Ednra*$^{Hoxa3/GFP}$ (H) mice. (I-L) Lateral views of skeletons of wild-type (I), *Ednra*$^{Hoxa3/+}$ (J), *Ednra*$^{GFP/GFP}$ (K) and *Ednra*$^{Hoxa3/GFP}$ (L) mice. (M-P) Schemes of skeletal structures of lateral and ventral view of wild-type (M) and *Ednra*$^{Hoxa3/+}$ (N) mice, lateral view of *Ednra*$^{GFP/GFP}$ (O) and *Ednra*$^{Hoxa3/GFP}$ (P) mice. Maxillary components are colored purple and mandibular ones are colored red.

A Fold difference of gene expression level	<-2.0	-2.0~-1.5	-1.5~-1.3	-1.3~-1.0	1.0~1.3	1.3~1.5	1.5~2.0	2.0<
Hoxa2 effects on maxillary process (d/a)	76	136	269	8378	9959	458	177	79
Hoxa2 effects on mandibular process (e/b)	11	79	428	10294	8406	232	55	27
Hoxa2 effects on PA2 (f/c)	11	38	242	9845	9151	191	44	10

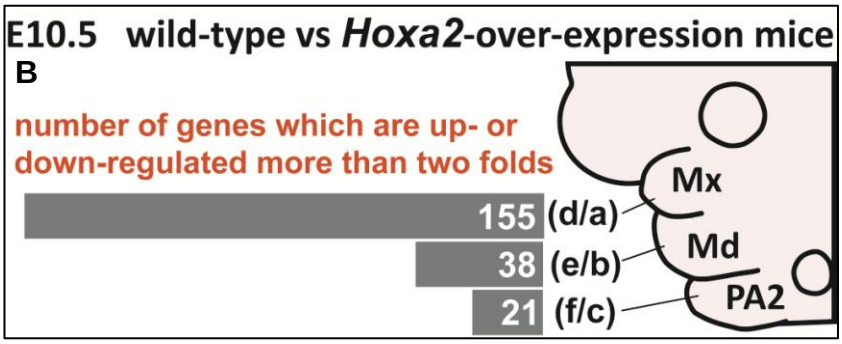

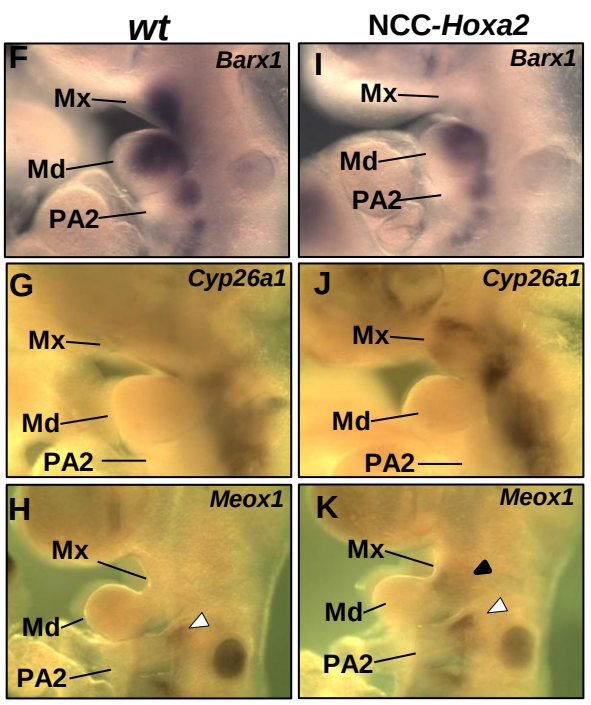

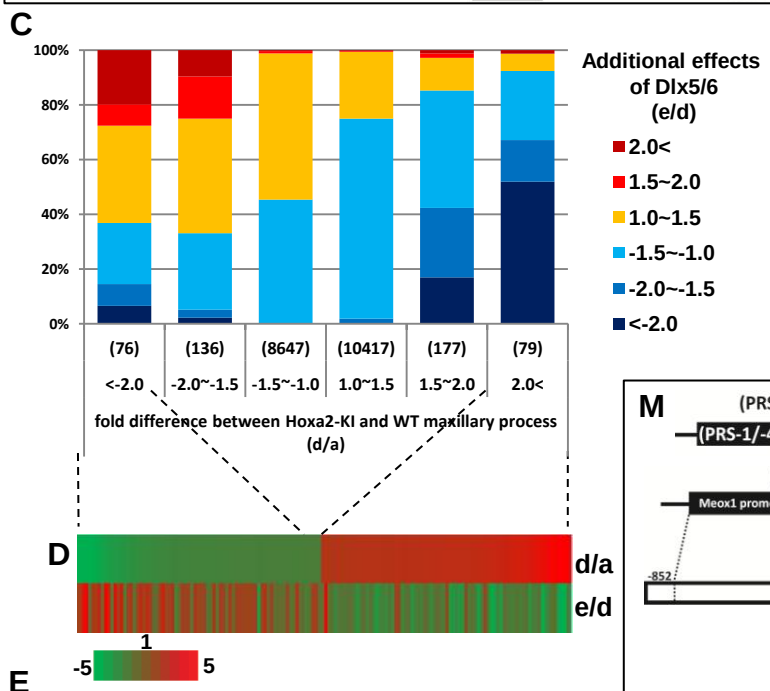

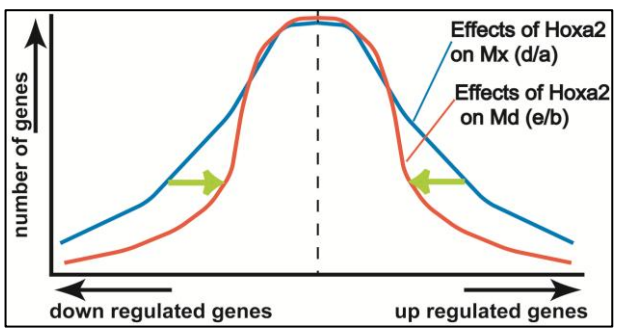

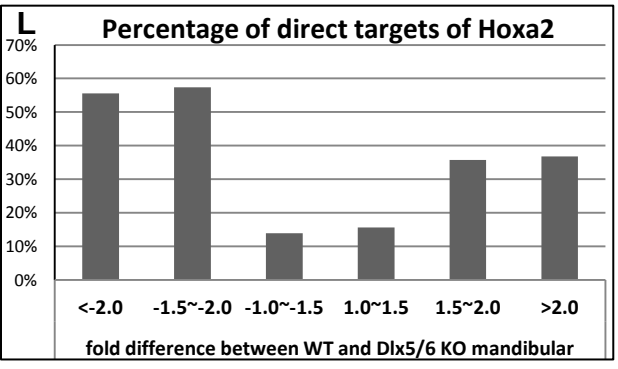

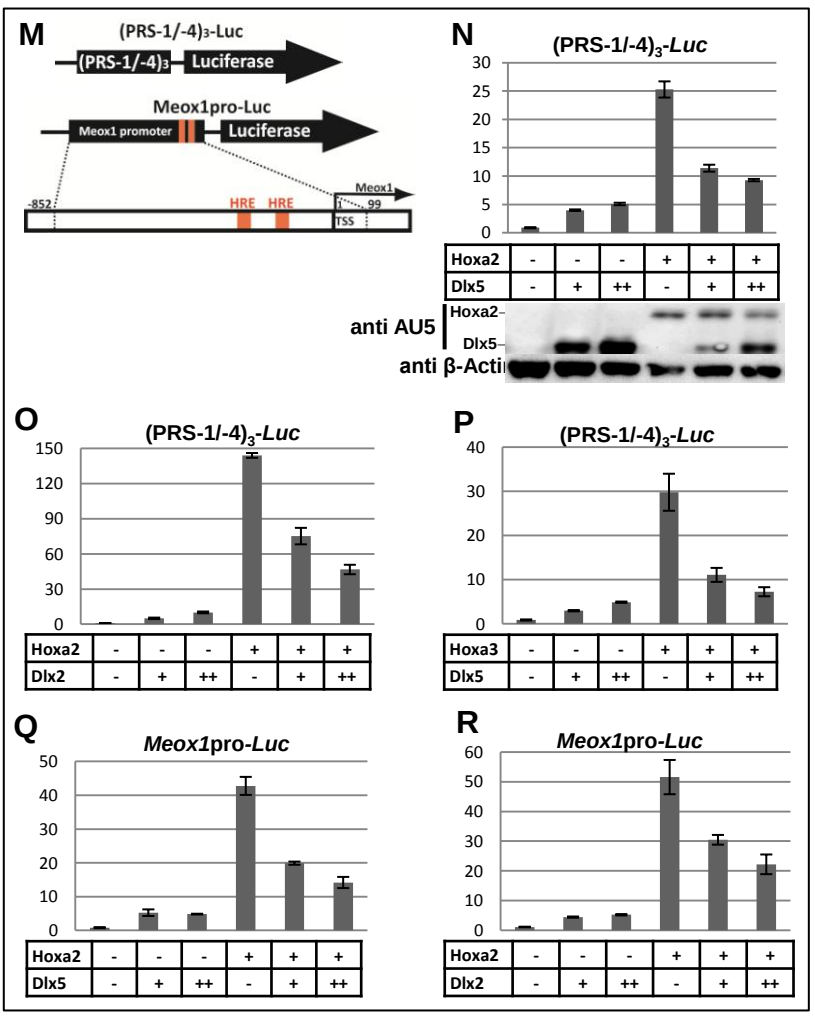

Figure 13. Hox and Dlx proteins show competition on gene regulation.
(A) A table indicating gene number distribution affected by over-expression of *Hoxa2* in the maxillary process (d/a), the mandibular process (e/b) and the PA2 (f/c), respectively. (B) Number of genes which are up- or down-regulated more than two-folds by ectopic *Hoxa2* in the maxillary process (d/a), mandibular process (e/b), and PA1 (f/c) respectively. (C) Fractional analysis demonstrating antagonism of *Dlx5/6* against transcriptional activity of *Hoxa2*. In a horizontal axis, about 20,000 genes are divided into six fractions according to fold difference between the maxillary process of NCC-*Hoxa2* and wild-type mice (d/a). Number of genes in each fraction is indicated in parentheses. Next, each fraction is further divided into six subfractions according to fold difference between the mandibular process and the maxillary process of NCC-*Hoxa2* mice (e/d), showing additional effects of *Dlx5/6*. (D) Heat maps indicationg additional effects of *Dlx5/6* against *Hoxa2*. Genes up-regulated or down-regulated more than two holds by *Hoxa2* are aligned in the top row (d/a), and additional effects of *Dlx5/6* against these genes are shown in the bottom row (e/d). (E) Schematic representation of gene number distribution affected by *Hoxa2*. Horizontal axis is the change of gene expression level, and vertical axis is gene number. Fewer genes are affected in mandibular context than in maxillary context. (F-K) Whole mount in situ hybridization of wild-type (F-H) and NCC-*Hoxa2* (I-K) mice for *Barx1* (E10.5) (F, I), *Cyp26a1* (E10.5) (G, J) and *Meox1* (E10.5) (H, K).Expression of *Meox1* in the PA2 and the PA1 is indicated by black and white arrow heads respectively. (L) Genes are divided into six groups according to fold difference between the mandibular process of wild-type and *Dlx5/6*$^{-/-}$mice, and percentage of Hoxa2 direct targets are calculated according to ChIP-seq data. HRE, Hox responsive element. (M) Scheme of construct of luciferase reporters. (N-R) Promoter assay using (*PRS-1/-4*)$_3$-Luc or *Meox1*pro-Luc in P19 cells. In (N), Hoxa2 and Dlx5 are tagged by AU5 peptide, and their expression level is indicated by western blotting.

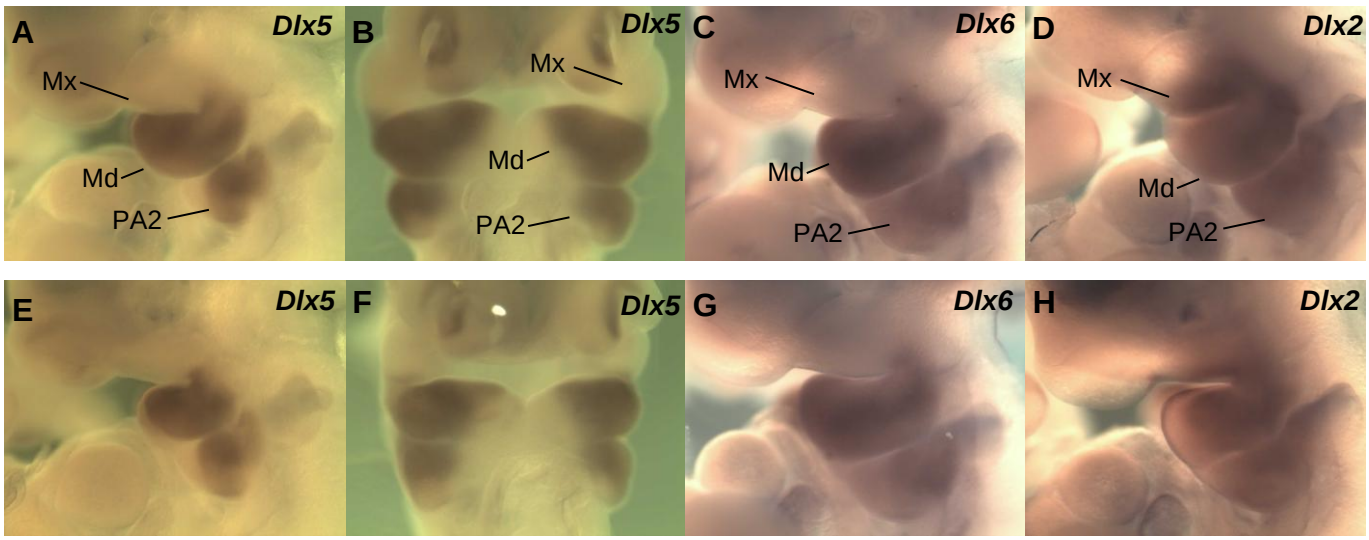

I	*Dlx5*	*Dlx6*	*Dlx2*
wt Mx vs NCC-*Hoxa2* Mx	**1.13**	**-1.03**	**1.38**
wt Md vs NCC-*Hoxa2* Md	**1.13**	**1.23**	**-1.04**
wt PA2 vs NCC-*Hoxa2*PA2	**1.08**	**1.03**	**1.21**

Figure 14. Expression pattern of Dlx genes in Hoxa2-over-expression mice
(A-H) Whole mount in situ hybridization against *Dlx5* (A, B, E, F), *Dlx6* (C, G) and *Dlx2* (D, H) in E10.5 wild-type (A-D) and NCC-*Hoxa2* (E-H) embryos. Lateral views (A, C, D, E, G, H) and frontal views (B, F). (I) Fold-change of expression level of *Dlx* genes between wild-type and NCC-*Hoxa2*.

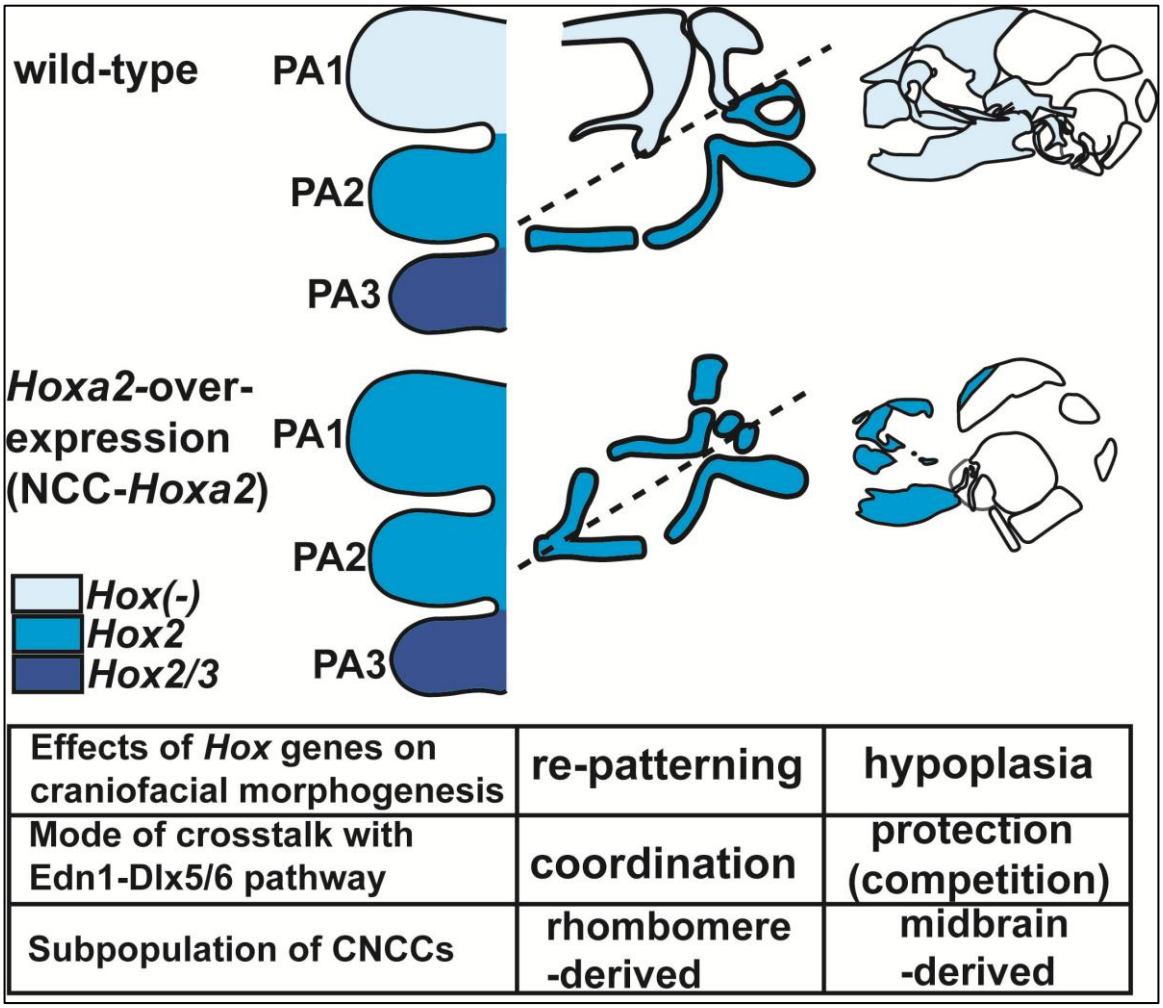

Effects of *Hox* genes on craniofacial morphogenesis	re-patterning	hypoplasia
Mode of crosstalk with Edn1-Dlx5/6 pathway	coordination	protection (competition)
Subpopulation of CNCCs	rhombomere -derived	midbrain -derived

Figure15. The summary of phenotype of *Hox* over-expression mice.
Ectopically expressed *Hox* genes in CNCCs induced two types of phenotype: structures originated from rhombomere-derived CNCCs showed re-patterning from PA1 to PA2, and structures originated from midbrain-derived CNCCs showed hypoplasia. The crosstalk between *Hox* genes and Edn1-Dlx5/6 pathway also showed dual modes, coordination and protection (competition).

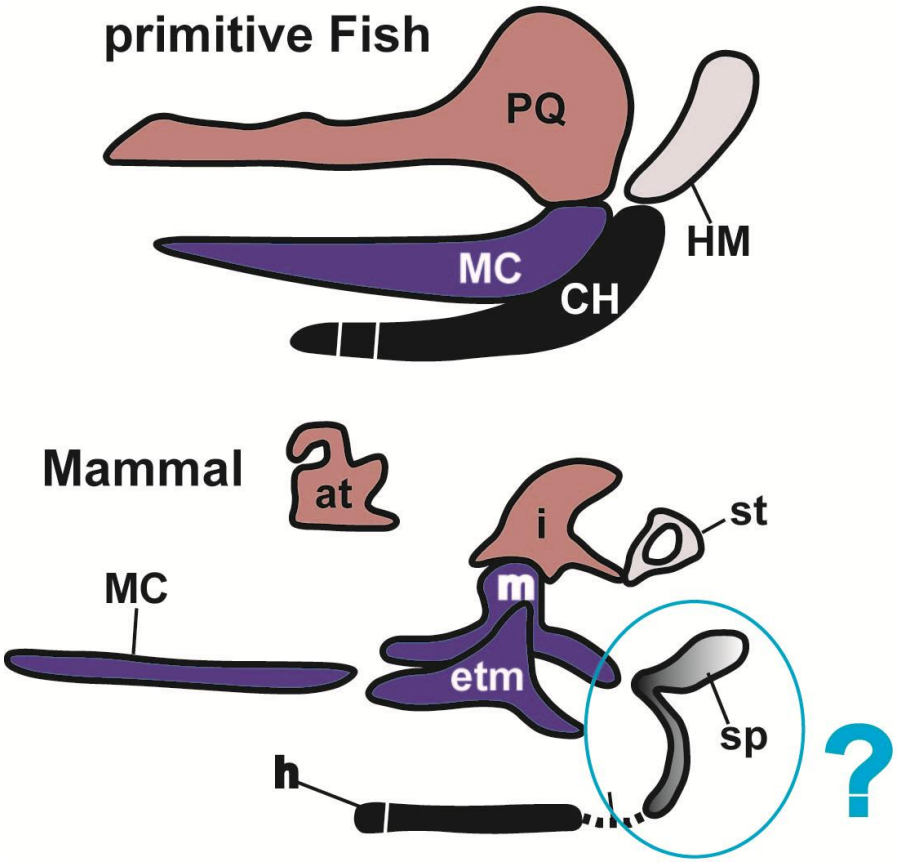

Figure 16. Evolutionary and developmental origin of the syloid process
PA2 of elasmobranchs mainly consists of the dorsal hyomandibular and the ventral ceratohyal componets. The styloid process is a PA2-derived mammalian-specific skeletal strucuture, but its evolutionary and developmental origins have not been dissected enough. at, ala temponalris; CH, ceratohyal; HM, hyomanidular; PQ, palatoquadrate.

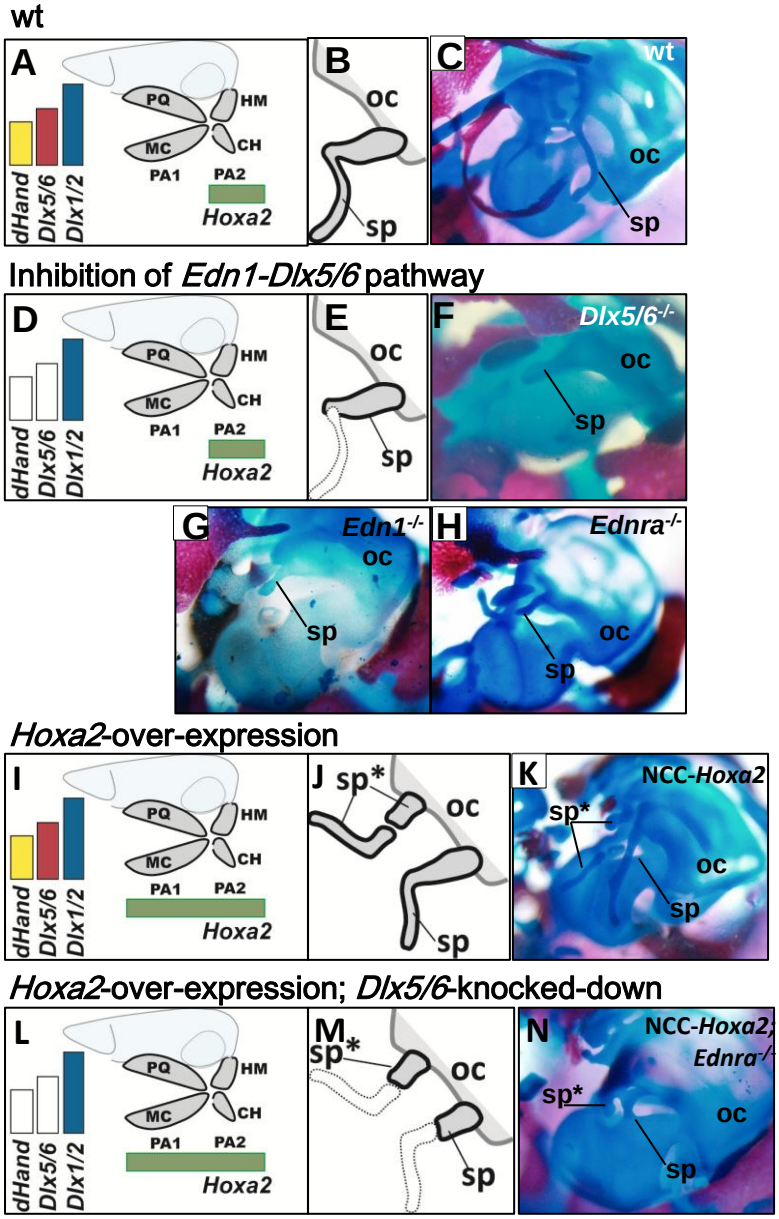

Figure 17. *Edn1-Dlx5/6* cascade is necessary for generation of the distal part of the styloid process. (A, D, I, L) Expression pattern of *Hox/ Dlx* genes in pharyngeal arches. (B, E, J, M) Shematic representation of the phenotypes of the styloid process. (C, F, G, H, K, N) Left lateral side around the middle ear of wild-type (C), *Dlx5/6*-null (F), *Edn1*-null (G), *Ednra*-null (H), NCC-*Hoxa2* (K) and NCC-*Hoxa2; Ednra*-null (N) mice. Embryonic stages of specimens are E17.5 or E18.5. CH, ceratohyal; HM, hyomandibular; MC; Meckel's cartilage; PQ, palatoquadrate; oc, otic capsule; sp, styloid process; *, duplicated structures.

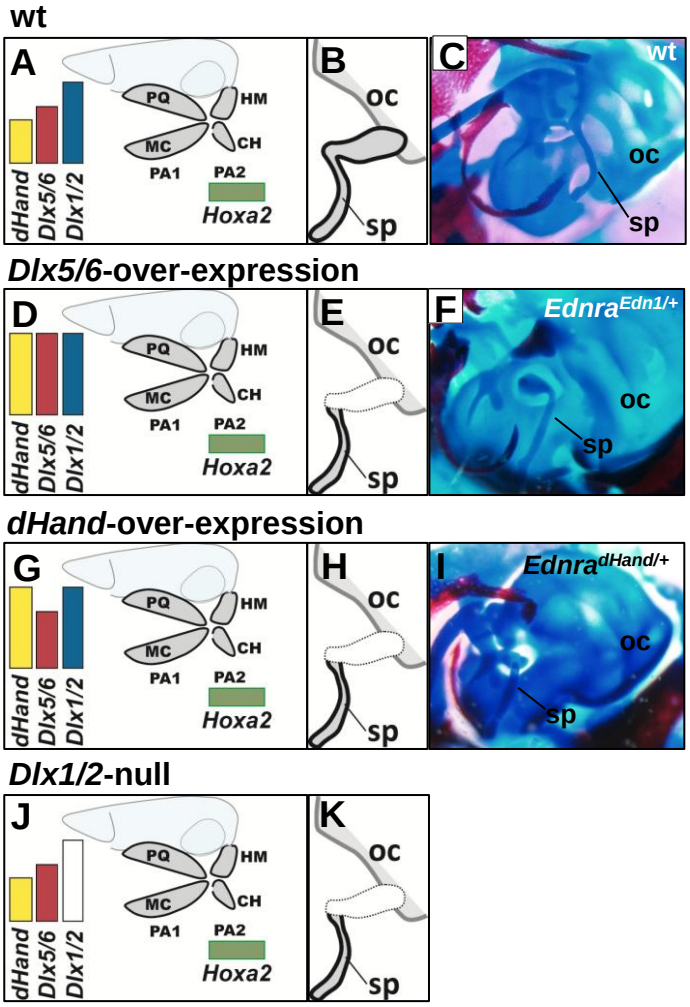

Figure 18. The proximal part of the styloid process is generated from *Edn1-Dlx5/6*-negative CNCCs. (A, D, G, J) Expression pattern of *Hox/ Dlx* genes in pharyngeal arches. (B, E, H, K) Shematic representation of the phenotypes of the styloid process. (C, F, I) Left lateral side around the middle ear of wild-type (C), *Edn1*-over-expression (F), and *dHand*-expression (I) mice. Embryonic stages of C and F are E18.5, and I is E15.5.

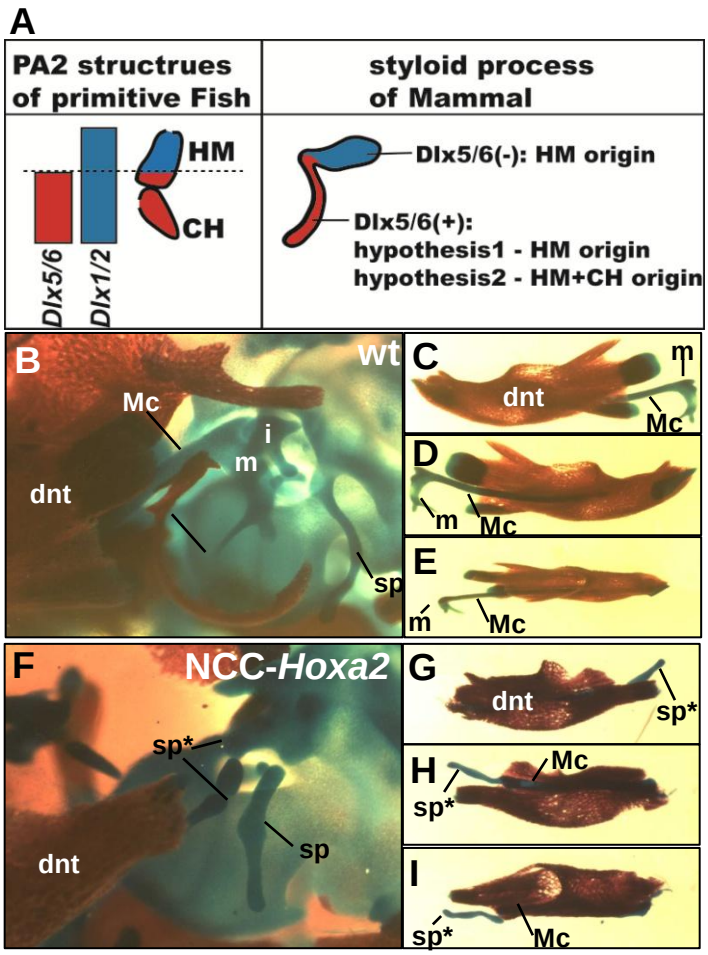

Figure 19. The distal part of the styloid process is serial homologue of the Meckel's cartilage. (A) Two types of working hypotheses for evolutionary and developmental origin of the distal part of the styloid process. (B, F) Left lateral side around the middle ear of E17.5 wild-type (B) and NCC-*Hoxa2* (F) mice. (C-E, G-I) Lateral (C, G), medial (D, H), and dorsal (E, I) of the left dentary bone. dnt, dentary bone; m, malleus; i, incus; Mc. Meckel's cartilage.

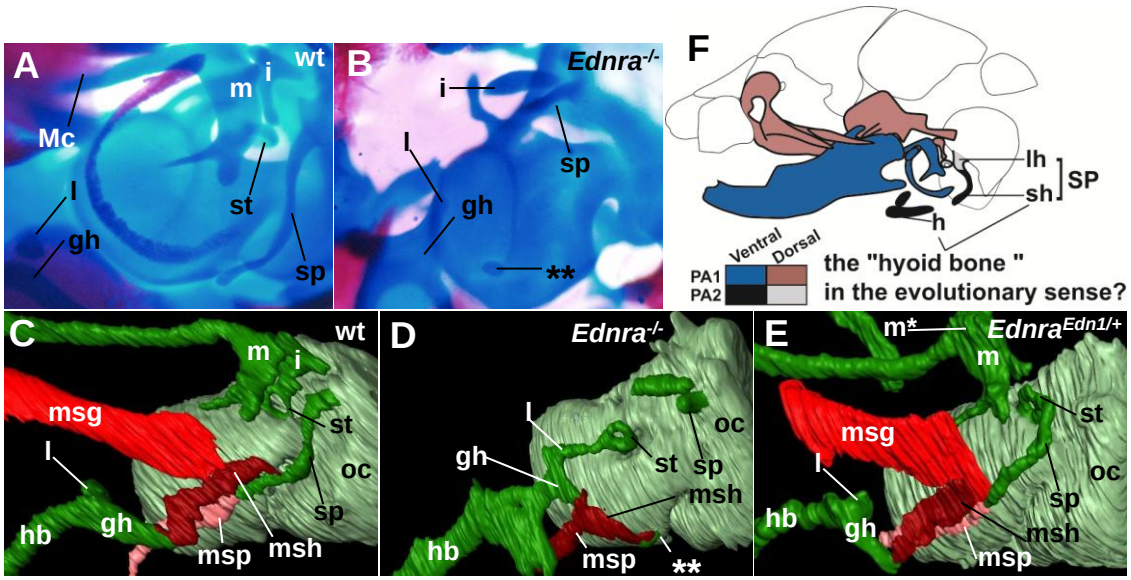

Figure 20. The distal part of the styloid process is the anchor point for muscle attachment. (A, B) Left lateral side around the middle ear of wild-type (A) and *Ednra*-null (B) mice. (C-E) Three-dimensional reconstruction of musculatures and skeletal structures of E17.5 wild-type (C), *Ednra*-null (D) and E18.5 *Edn1*-over-expression (E) mice. Skeletal structures are colored by green while musculatures are colored by red, brown, or pink. (F) Shematic representation of evolutionary dual origins of the styloid process. gh, greater horn of the hyoid bone; hb, hyoid body; l, lesser horn of the hyoid bone; lh, laterohyal; msg, styloglossal muscle; msh, stylohyal muscle; msp, stylopharyngeal muscle; ost, otostapes; sh, stylohyal; SP, styloid process; st, stapes; **, condensed cartilage.

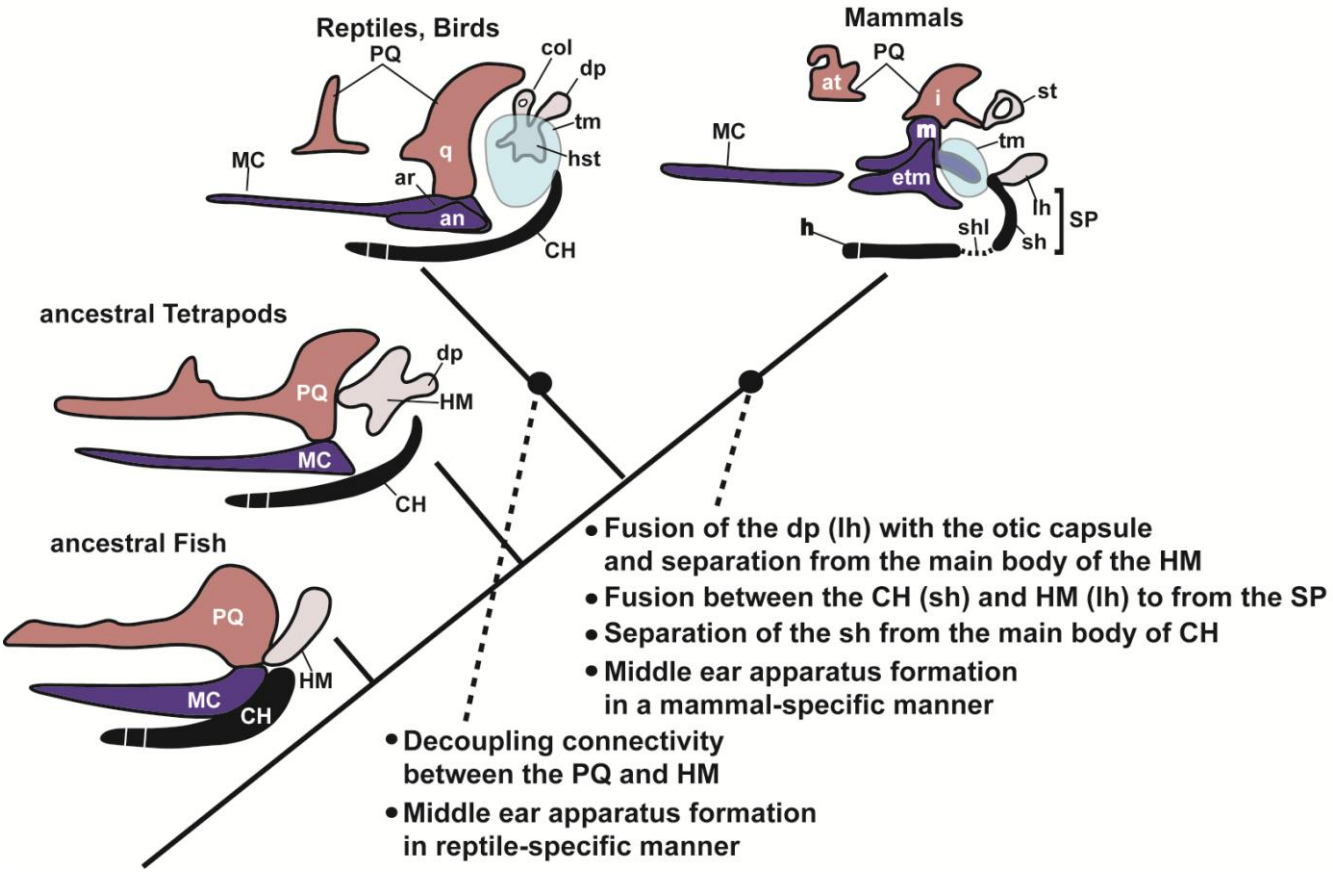

Figure 21. The cladogram of evolution of the middle ear of mammals.
an, angular; at, alatempolaris; col, columella; dp, dorsal process; etm, ectotympanic ring; h, hyoid bone; hst, hyostpes; q, quadrate; shl, stylohyal ligament; tm, tympanic membrane.

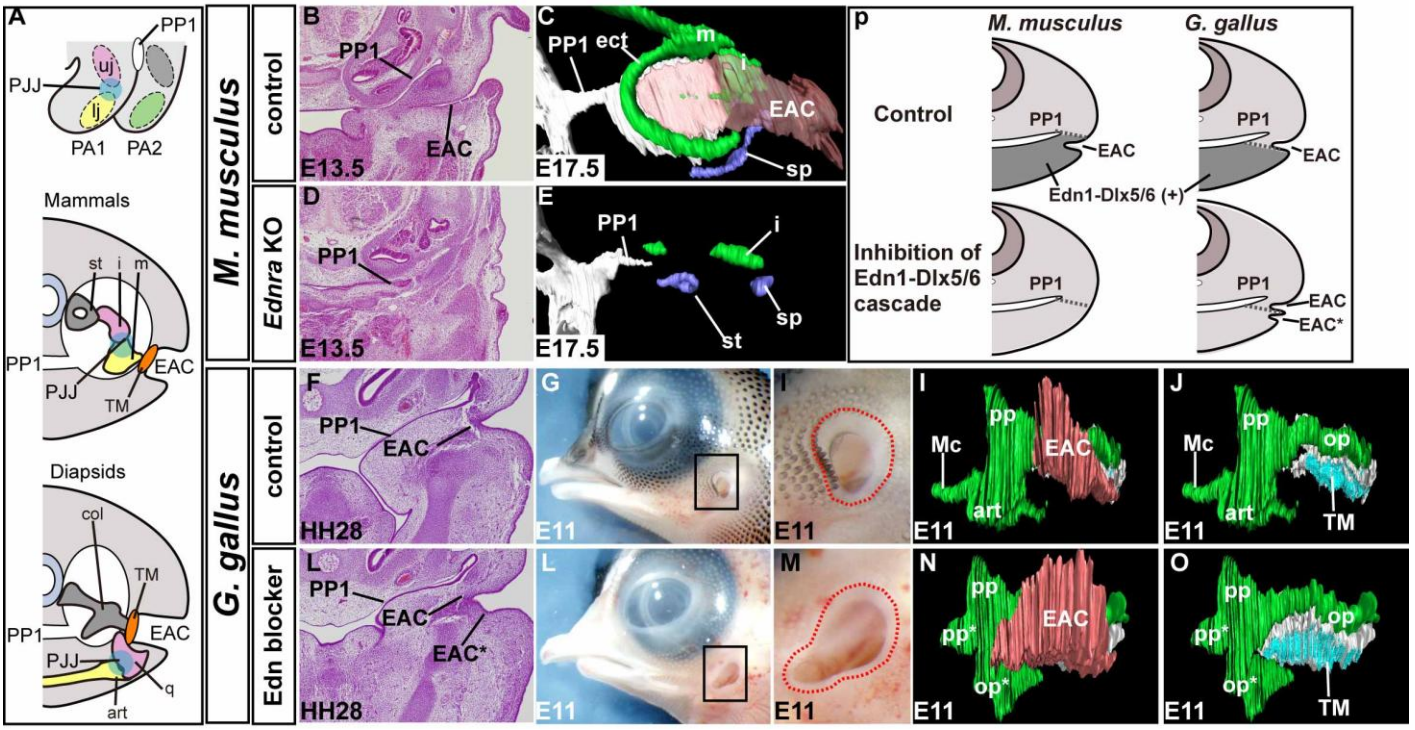

Figure 22. Comparison of middle ear phenotypes induced by inhibition of Edn1-Dlx5/6 cascade in the mouse and chicken.

A, Development and morphlogy of amniote middle ears. Generalized scheme of rostral pharyngeal arches in pharyngula shown in the left lateral view (top), transverse section of the mammalian middle ear (middle) and the diapsid middle ear (bottom). Three ear ossicles, malleus (m), incus (i), and stapes (st) are present in mammals, while diapsids have only one ossicle, columella auris (col). The malleus and incus are homologous to the elements forming the primary jaw joint (PJJ), the articular (art) and quadrate (q), respectively. **B** and **D**, Horizontal sections of control (**B**) and *Ednra*-null (**D**) mice. **C** and **E**, Left ventrolateral views of 3D reconstructed skeletons of the first (PA1; colored green) and second (PA2; blue) pharyngeal arches. The external auditory canal (EAC) is colored pink, and the first pharyngeal pouch (PP1) white. **F-O**, Control (**F-J**) and edn1-blocker treated (**K-O**) chickens. **F**and **K**, Horizontal sections. **G**, **H**, **L**, **M**, Left lateral views. **H** and **M**, Higher magnification of boxes in **G** and **L**, respectively. **I**, **J**, **N**, **O**, Three-dimensional reconstructions (the external auditory canal is removed in **J** and **O**), and the tympanic membrane (TM) is colored light blue. **P**, Summary of the induced middle ear phenotypes. etm, ectotympanic ring; lj, lower jaw; Mc, Meckel's cartilage; op, otic process of quadrate; pp, pterygoid process of quadrate; sp, styloid process; st, stapes; uj, upper jaw; * duplicated elements.

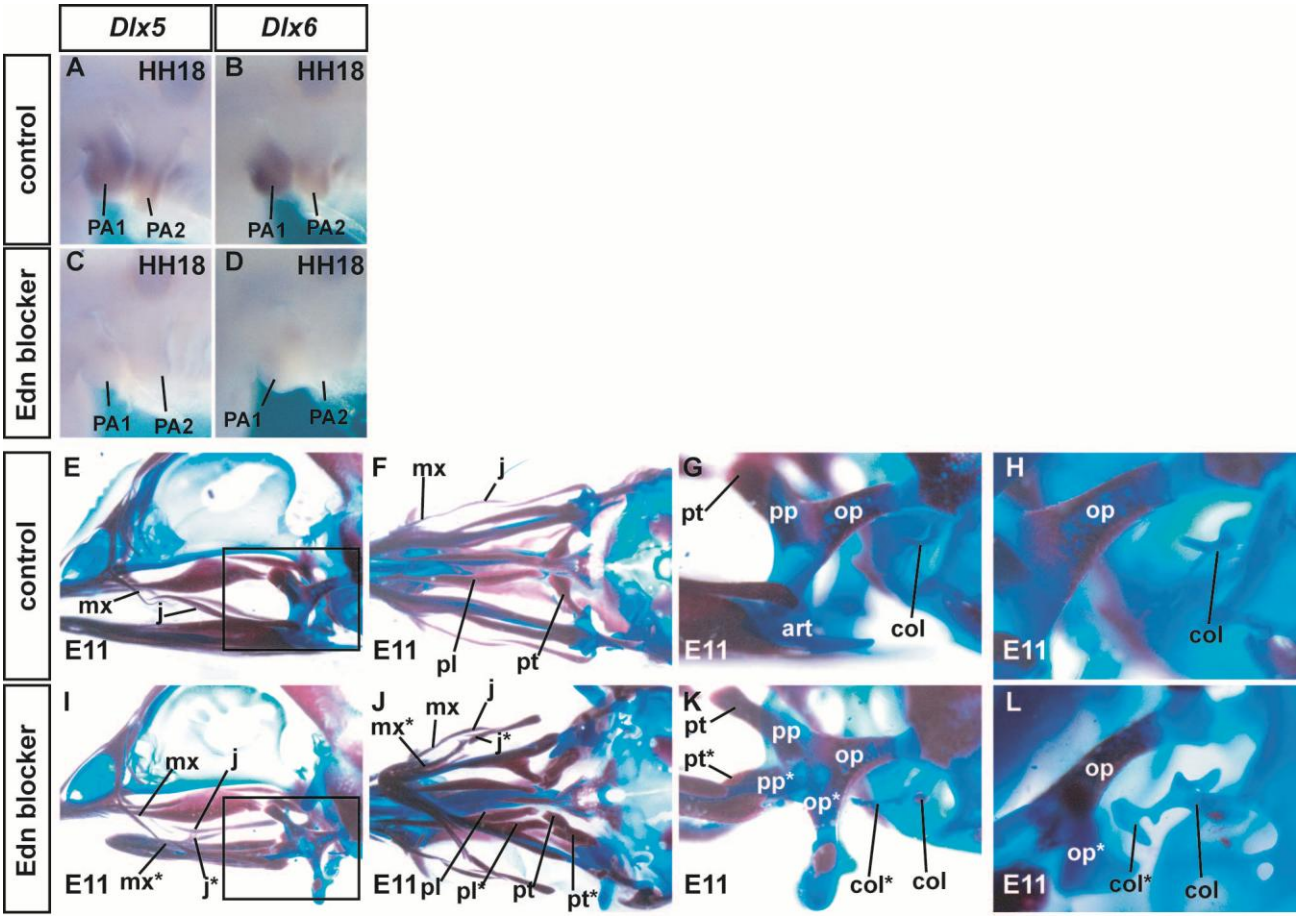

Figure 23. Treatment of Edn-blocker in chicks induces homeotic transformation of the lower jaw into upper jaw.

A-D, *In situ* hybridization of *Dlx5* (**A**, **C**), *Dlx6* (**B**, **D**) in pharyngeal arches of control (**A-B**) and Edn-blocker treated (**C-D**) chicken embryos. **E-L**, left lateral views (**E**, **G, I**, **K**), ventral views (**F**, **J**) and left ventrolateral views (**H**, **L**) of the control (**E-H**) and Edn-blocker treated (**I-L**) chicken. **G** and **K** are higher magnification of boxes in **E** and **I**, respectively.art, articular; j, jugal; mx, maxilla; op, otic process of quadrate; pp, pteryogid process of quadrate; pl, palatine; pt, pterygoid; *, duplicated elements.

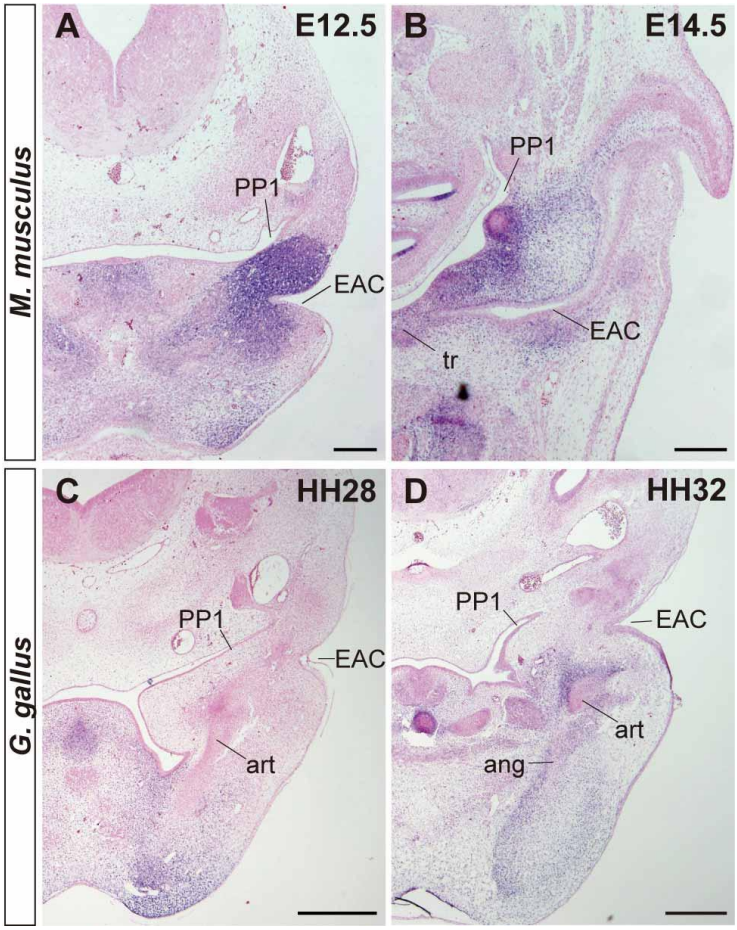

Figure 24. Expression pattern of Gsc in the chicken and mouse embryo. *Gsc* expression in transverse sections of the mouse (**A**, **B**) and chicken (**C**, **D**) embryos.

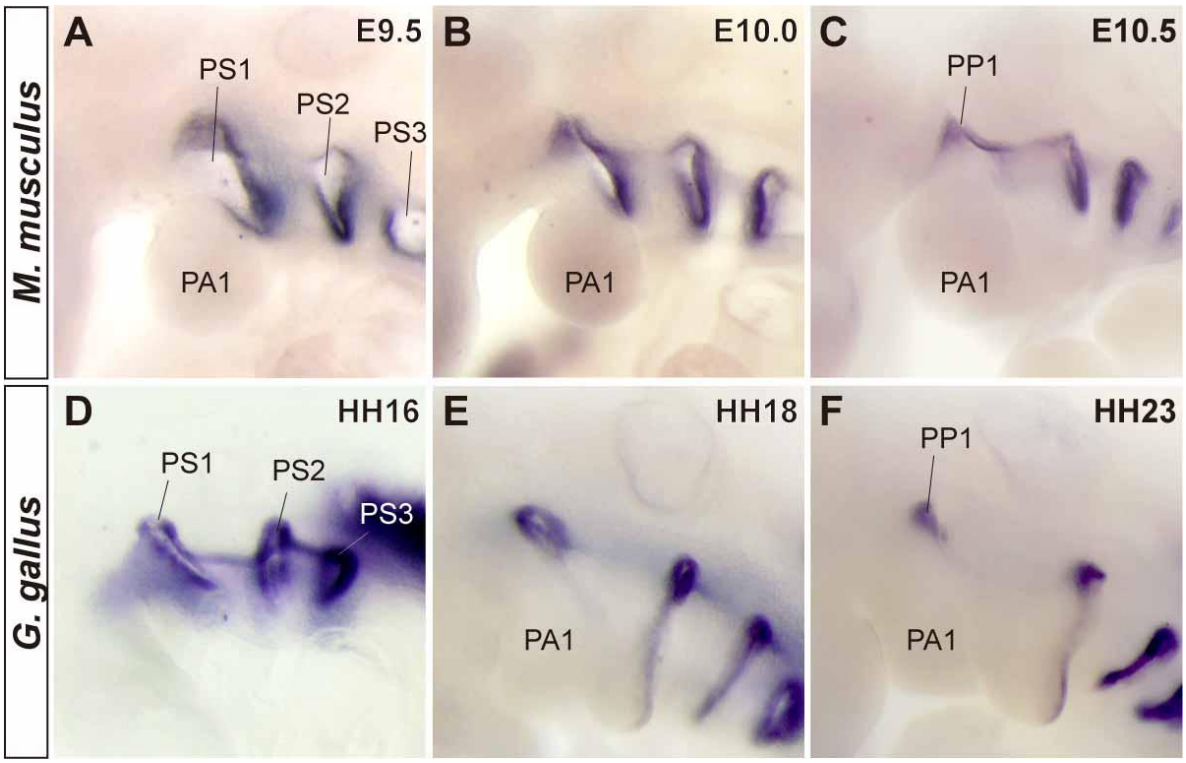

Figure 25. The development of the first pharygeal pouch in the mouse and chiken.
Pax1 expression in the pharyngeal slits in mouse (**A**-**C**) and chicken (**D**-**F**) embryos. PS1-3, pharyngeal slits 1-3.

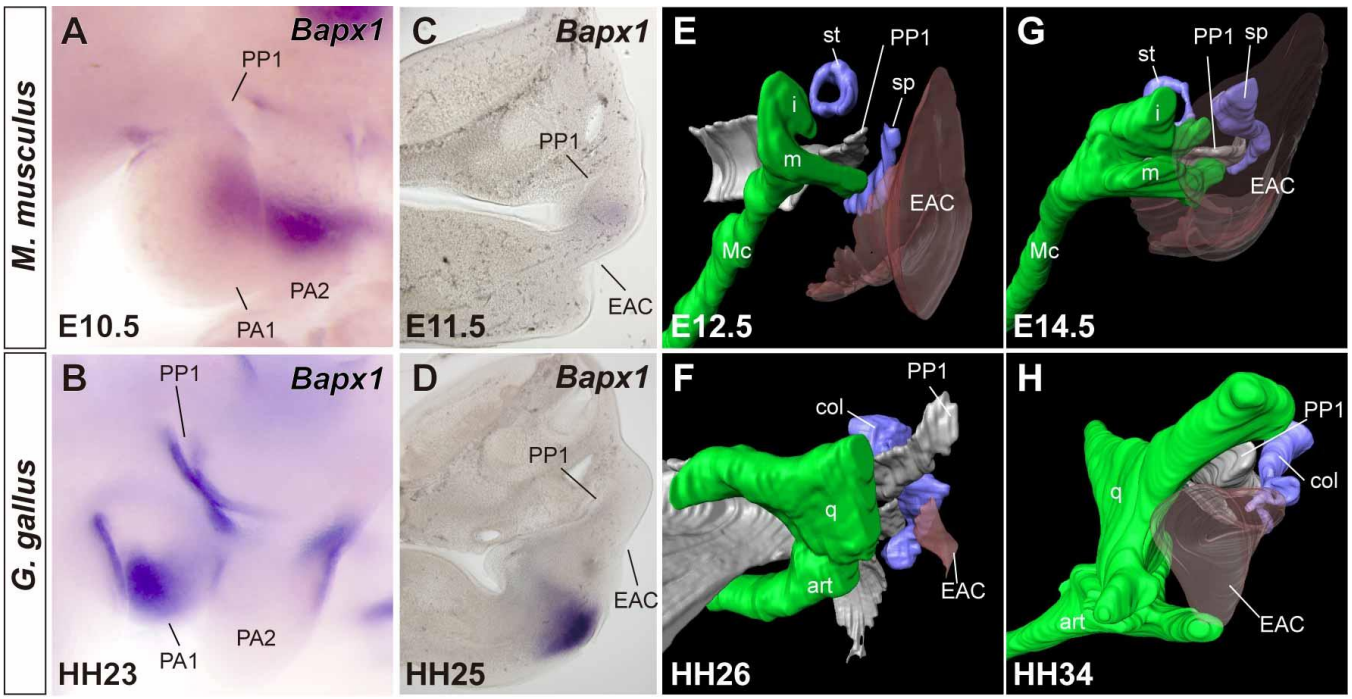

Figure 26. Comparison of development of the tympanic membrane and primary jaw joint in the mouse and chicken embryo.
A and **B**, *Bapx1* expression in the pharyngeal arches of the embryonic day 10.5 mouse and stage 23 chicken. **C** and **D**, *Bapx1* expression in the mouse and chicken embryo. **E**-**H**, Three-dimensional reconstruction of forming the pharyngeal skeleton and tympanic membrane based on histological sections of embryonic day 12.5 (**E**) and 14.5 (**G**) mouse, and stage 26 (**F**) and 34 (**H**) chicken. In the **E** and **F**, procartilaginous development was detected by *in situ* hybridization of *Aggrecan* expression.

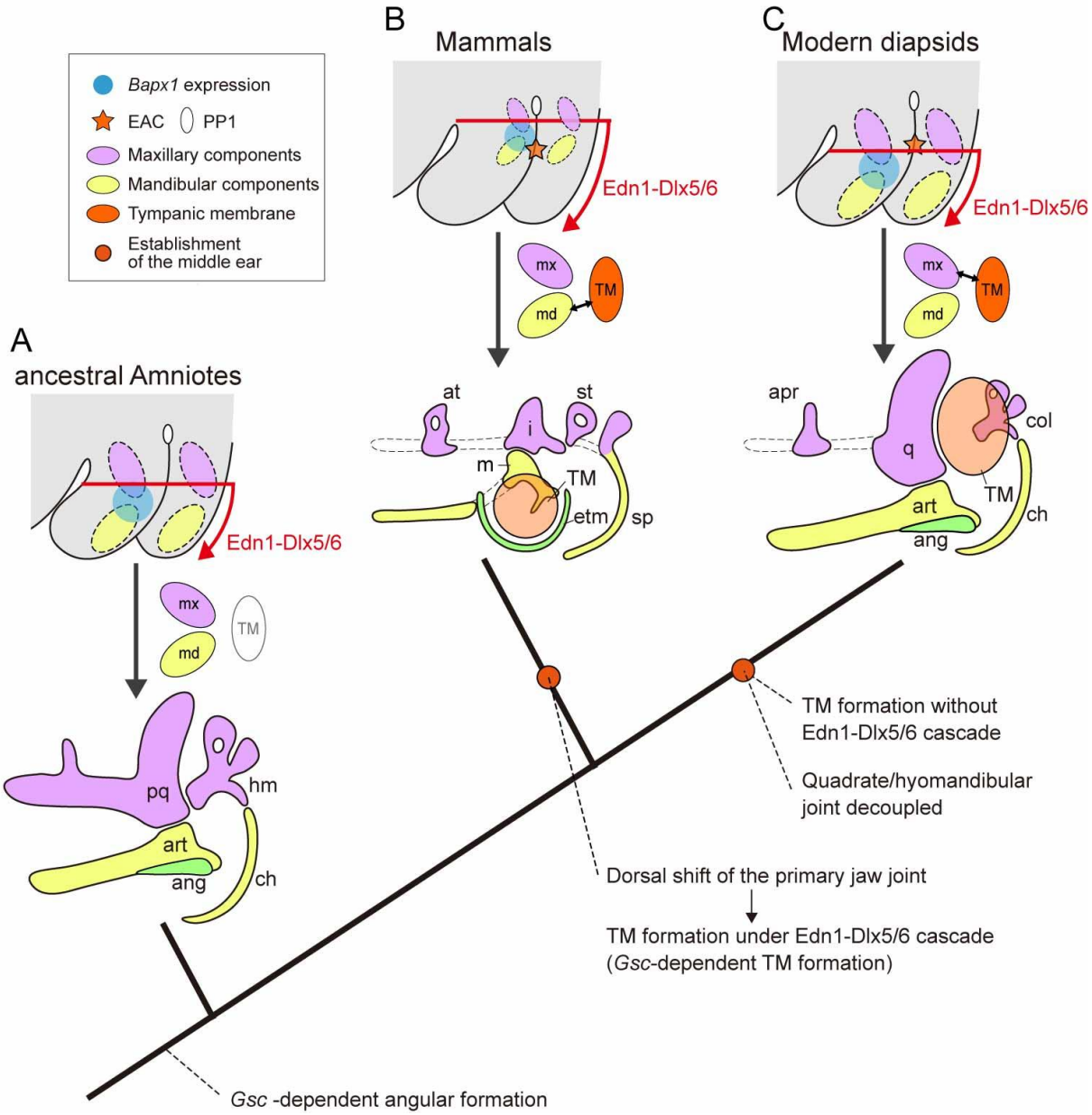

Figure 27. Hypothesized scenario of the tympanic membrane and middle ear evolution in amniotes.

A, In ancestral amniotes, the *Bapx1* expression (blue circle) or the position of PJJ, is thought to have been distant from PP1. The TM had not yet been obtained. **B**, In mammalian ancestors, PJJ shifts dorsally to the proximity of PP1, leading to the coupling of TM and lower jaw specifications to form Edn-Dlx5/6-dependent TM in the lower jaw domain. This TM spanns the angular, dependent on *Gsc* expression. **C**, In modern diapsids, the position of the PJJ retains the ancestral state. The hyomandibular was decoupled from the quadrate and established a connection with the Edn-Dlx5/6-independent TM in the upper jaw domain, which is coupled with the upper jaw. apr, ascending process; at, ala temporalis; ch, ceratohyal; hm, hyomandibular; pq, palatoquadrate.

Down regulation of *Hoxa2*	Santagati F, et al. (2005) [3]	Mouse	NCCs	Homeotic transformation (PA2→ PA1)
	Couly G, et al. (1998) [4]	Chick	NCCs	Homeotic transformation (PA2→ PA1)
	Baltzinger M, et al. (2005) [5]	Xenopus	NCCs & surrounding tissues	Homeotic transformation (PA2→ PA1)
	Hunter MP, et al. (2002) [6]	Zebrafish	NCCs & surrounding tissues	Homeotic transformation (PA2→ PA1)
Up regulation of *Hoxa2*	This study	Mouse	NCCs (CAG promoter)	Homeotic transformation (PA1→ PA2)
	This study	Mouse	NCCs (*Ednra* promoter)	No homeotic transformation
	Minoux M, et al. (2013) accepted	Mouse	NCCs (*ROSA26* promoter)	Duplication of auricles
	Massip L*, et al.* (2007) [7] & Tavella S, et al. (2010) [8]	Mouse	Chondrocytes	No homeotic transformation
	Creuzet S, et al. (2002) [9]	Chick	NCCs	No homeotic transformation
	Grammatopoulos GA, et al. (2002) [10]	Chick (chimera)	NCCs	No homeotic transformation
	Grammatopoulos GA, et al. (2002) [10]	Chick (retrovirus)	NCCs & surrounding tissues	Homeotic transformation (PA1→ PA2)
	Pasqualetti M, et al. (2000) [11]	Xenopus	NCCs & surrounding tissues	Homeotic transformation (PA1→ PA2)
	Hunter MP, et al. (2002) [6]	Zebrafish	NCCs & surrounding tissues	Homeotic transformation (PA1→ PA2)

Table 1Summary of *Hoxa2* down or up regulation analysis in pharyngeal arches

PA; pharyngeal arch.
NCCs; neural crest cells

ACKNOWLEDGMENTS.

I thank H. Kurihara, K. Fujisawa, Y. Arima, Y. Kawamura, Y. Uchijima, K. Nishiyama, Y. Kurihara, T. Sato, K. Kim, R. Asai, M. Shimizu, D. Seya, W. Isono, K. Maruyama, H. Kume, S. Kushiyama, Y. Fujisawa, Y Kondo and A Matsubara (the University of Tokyo, Tokyo, Japan) for experimental support; S. Kuratani (RIKEN Center for Developmental Biology, Kobe, Japan) and M. Takechi (Iwate Medical University, Iwate, Japan) for helpful discussion about the tympanic membrane; F. M. Rijli, M. Minoux (Freidrich Miexcher Institute for Biomedical Research, Basel, Swizerland), G. Levi and N, Narboux- Nême (Muséum National d'Histoire Naturelle, Paris, France) for analysis of mutant mice; S. Miyagawa-Tomita and K. Maeda for analysis of bosentan-treated chicken embryos; K. Yamamura (Kumamoto University, Kumamoto,Japan) and K. Araki (Kumamoto University, Kumamoto, Japan) for *lox*-containing plasmids; I. Saito (University of Tokyo, Tokyo) for Creexpressing adenovirus; T. Kodama, H. Aburatani, Y. Wada, T. Inoue, T. Kohro, A. Taguchi. K. Kaneki and M. Kobayashi (Research Center for Advanced Science and Technology, Tokyo, Japan) for microarray experiments; My gratitude is extended to Actelion Pharmaceuticals Ltd for the bosentan usage. T. Kitazawa is a Research Fellow of the Japan Society for the Promotion of Science (DC2).

References

1. Asai R, Kurihara Y, Fujisawa K, Sato T, Kawamura Y, et al. (2010) Endothelin receptor type A expression defines a distinct cardiac subdomain within the heart field and is later implicated in chamber myocardium formation. Development 137: 3823-3833.

2. Kurihara Y, Kurihara H, Suzuki H, Kodama T, Maemura K, et al. (1994) Elevated blood pressure and craniofacial abnormalities in mice deficient in endothelin-1. Nature 368: 703-710.

3. Beverdam A, Merlo GR, Paleari L, Mantero S, Genova F, et al. (2002) Jaw transformation with gain of symmetry after Dlx5/Dlx6 inactivation: mirror of the past? Genesis 34: 221-227.

4. Sato T, Kurihara Y, Asai R, Kawamura Y, Tonami K, et al. (2008) An endothelin-1 switch specifies maxillomandibular identity. Proc Natl Acad Sci U S A 105: 18806-18811.

5. Chai Y, Jiang X, Ito Y, Bringas P, Jr., Han J, et al. (2000) Fate of the mammalian cranial neural crest during tooth and mandibular morphogenesis. Development 127: 1671-1679.

6. Sato T, Kawamura Y, Asai R, Amano T, Uchijima Y, et al. (2008) Recombinase-mediated cassette exchange reveals the selective use of Gq/G11-dependent and -independent endothelin 1/endothelin type A receptor signaling in pharyngeal arch development. Development 135: 755-765.

7. Araki K, Araki M, Yamamura K (2002) Site-directed integration of the cre gene mediated by Cre recombinase using a combination of mutant lox sites. Nucleic Acids Res 30: e103.

8. Kanegae Y, Lee G, Sato Y, Tanaka M, Nakai M, et al. (1995) Efficient gene activation in mammalian cells by using recombinant adenovirus expressing site-specific Cre recombinase. Nucleic Acids Res 23: 3816-3821.

9. McLeod MJ (1980) Differential staining of cartilage and bone in whole mouse fetuses by alcian blue and alizarin red S. Teratology 22: 299-301.

10. Arima Y, Miyagawa-Tomita S, Maeda K, Asai R, Seya D, et al. (2012) Preotic neural crest cells contribute to coronary artery smooth muscle involving endothelin signalling. Nat Commun 3: 1267.

11. Wilkinson DG (1992) In situ hybridization : a practical approach. Oxford: IRL Press at Oxford University Press. xvii, 163 p. p.

12. Murakami M, Tominaga J, Makita R, Uchijima Y, Kurihara Y, et al. (2006)

Transcriptional activity of Pax3 is co-activated by TAZ. Biochem Biophys Res Commun 339: 533-539.

13. Kirilenko P, He G, Mankoo BS, Mallo M, Jones R, et al. (2011) Transient activation of meox1 is an early component of the gene regulatory network downstream of hoxa2. Mol Cell Biol 31: 1301-1308.

14. Murga C, Laguinge L, Wetzker R, Cuadrado A, Gutkind JS (1998) Activation of Akt/protein kinase B by G protein-coupled receptors. A role for alpha and beta gamma subunits of heterotrimeric G proteins acting through phosphatidylinositol-3-OH kinasegamma. J Biol Chem 273: 19080-19085.

15. Kim KS, Arima Y, Kitazawa T, Nishiyama K, Asai R, et al. (2013) Endothelin regulates neural crest deployment and fate to form great vessels through Dlx5/Dlx6-independent mechanisms. Mech Dev.

16. Kempf H, Linares C, Corvol P, Gasc JM (1998) Pharmacological inactivation of the endothelin type A receptor in the early chick embryo: a model of mispatterning of the branchial arch derivatives. Development 125: 4931-4941.

17. Carroll SB (1995) Homeotic genes and the evolution of arthropods and chordates. Nature 376: 479-485.

18. Akam M (1989) Hox and HOM: homologous gene clusters in insects and

vertebrates. Cell 57: 347-349.

19. Akam M (1991) Developmental biology. Wondrous transformation. Nature 349: 282.

20. McGinnis W, Krumlauf R (1992) Homeobox genes and axial patterning. Cell 68: 283-302.

21. Le Douarin NM (2004) The avian embryo as a model to study the development of the neural crest: a long and still ongoing story. Mech Dev 121: 1089-1102.

22. Minoux M, Rijli FM (2010) Molecular mechanisms of cranial neural crest cell migration and patterning in craniofacial development. Development 137: 2605-2621.

23. Rijli FM, Mark M, Lakkaraju S, Dierich A, Dolle P, et al. (1993) A homeotic transformation is generated in the rostral branchial region of the head by disruption of Hoxa-2, which acts as a selector gene. Cell 75: 1333-1349.

24. Gendron-Maguire M, Mallo M, Zhang M, Gridley T (1993) Hoxa-2 mutant mice exhibit homeotic transformation of skeletal elements derived from cranial neural crest. Cell 75: 1317-1331.

25. Chisaka O, Capecchi MR (1991) Regionally restricted developmental defects resulting from targeted disruption of the mouse homeobox gene hox-1.5. Nature

350: 473-479.

26. Santagati F, Minoux M, Ren SY, Rijli FM (2005) Temporal requirement of Hoxa2 in cranial neural crest skeletal morphogenesis. Development 132: 4927-4936.

27. Pasqualetti M, Ori M, Nardi I, Rijli FM (2000) Ectopic Hoxa2 induction after neural crest migration results in homeosis of jaw elements in Xenopus. Development 127: 5367-5378.

28. Grammatopoulos GA, Bell E, Toole L, Lumsden A, Tucker AS (2000) Homeotic transformation of branchial arch identity after Hoxa2 overexpression. Development 127: 5355-5365.

29. Creuzet S, Couly G, Vincent C, Le Douarin NM (2002) Negative effect of Hox gene expression on the development of the neural crest-derived facial skeleton. Development 129: 4301-4313.

30. Couly G, Grapin-Botton A, Coltey P, Ruhin B, Le Douarin NM (1998) Determination of the identity of the derivatives of the cephalic neural crest: incompatibility between Hox gene expression and lower jaw development. Development 125: 3445-3459.

31. Depew MJ, Lufkin T, Rubenstein JL (2002) Specification of jaw subdivisions by Dlx genes. Science 298: 381-385.

32. Ozeki H, Kurihara Y, Tonami K, Watatani S, Kurihara H (2004) Endothelin-1 regulates the dorsoventral branchial arch patterning in mice. Mech Dev 121: 387-395.

33. Ruest LB, Xiang X, Lim KC, Levi G, Clouthier DE (2004) Endothelin-A receptor-dependent and -independent signaling pathways in establishing mandibular identity. Development 131: 4413-4423.

34. Santagati F, Rijli FM (2003) Cranial neural crest and the building of the vertebrate head. Nat Rev Neurosci 4: 806-818.

35. Creuzet S, Schuler B, Couly G, Le Douarin NM (2004) Reciprocal relationships between Fgf8 and neural crest cells in facial and forebrain development. Proceedings of the National Academy of Sciences of the United States of America 101: 4843-4847.

36. Donaldson IJ, Amin S, Hensman JJ, Kutejova E, Rattray M, et al. (2012) Genome-wide occupancy links Hoxa2 to Wnt-beta-catenin signaling in mouse embryonic development. Nucleic Acids Res 40: 3990-4001.

37. Hunter MP, Prince VE (2002) Zebrafish hox paralogue group 2 genes function redundantly as selector genes to pattern the second pharyngeal arch. Dev Biol 247: 367-389.

38. Baltzinger M, Ori M, Pasqualetti M, Nardi I, Rijli FM (2005) Hoxa2 knockdown in Xenopus results in hyoid to mandibular homeosis. Dev Dyn 234: 858-867.

39. Kontges G, Lumsden A (1996) Rhombencephalic neural crest segmentation is preserved throughout craniofacial ontogeny. Development 122: 3229-3242.

40. Couly G, Grapin-Botton A, Coltey P, Le Douarin NM (1996) The regeneration of the cephalic neural crest, a problem revisited: the regenerating cells originate from the contralateral or from the anterior and posterior neural fold. Development 122: 3393-3407.

41. Miller CT, Maves L, Kimmel CB (2004) moz regulates Hox expression and pharyngeal segmental identity in zebrafish. Development 131: 2443-2461.

42. Schilling TF, Kimmel CB (1994) Segment and cell type lineage restrictions during pharyngeal arch development in the zebrafish embryo. Development 120: 483-494.

43. Couly G, Creuzet S, Bennaceur S, Vincent C, Le Douarin NM (2002) Interactions between Hox-negative cephalic neural crest cells and the foregut endoderm in patterning the facial skeleton in the vertebrate head. Development 129: 1061-1073.

44. Noyes MB, Christensen RG, Wakabayashi A, Stormo GD, Brodsky MH, et al.

(2008) Analysis of homeodomain specificities allows the family-wide prediction of preferred recognition sites. Cell 133: 1277-1289.

45. Takechi M, Kuratani S (2010) History of studies on mammalian middle ear evolution: a comparative morphological and developmental biology perspective. J Exp Zool B Mol Dev Evol 314: 417-433.

46. Anthwal N, Joshi L, Tucker AS (2013) Evolution of the mammalian middle ear and jaw: adaptations and novel structures. J Anat 222: 147-160.

47. Goodrich ES (1930) Studies on the structure & development of vertebrates. London,: Macmillan and co., limited. xxx, 837 p. p.

48. De Beer G (1937) The development of the vertebrate skull. Oxford,: Clarendon Press. xxiii, 552 p. p.

49. Wilczynski W (1992) The Evolutionary Biology of Hearing - Webster,Db, Fay,Rr, Popper,An. Nature 358: 202-202.

50. O'Gorman S (2005) Second branchial arch lineages of the middle ear of wild-type and Hoxa2 mutant mice. Dev Dyn 234: 124-131.

51. Gillis JA, Modrell MS, Baker CV (2013) Developmental evidence for serial homology of the vertebrate jaw and gill arch skeleton. Nat Commun 4: 1436.

52. Medeiros DM (2013) The evolution of the neural crest: new perspectives from

lamprey and invertebrate neural crest-like cells. Wiley Interdiscip Rev Dev Biol 2: 1-15.

53. Qiu M, Bulfone A, Ghattas I, Meneses JJ, Christensen L, et al. (1997) Role of the Dlx homeobox genes in proximodistal patterning of the branchial arches: mutations of Dlx-1, Dlx-2, and Dlx-1 and -2 alter morphogenesis of proximal skeletal and soft tissue structures derived from the first and second arches. Dev Biol 185: 165-184.

54. Minoux M, Kratochwil CF, Ducret S, Amin S, Kitazawa T, et al. (2013) Mouse Hoxa2 mutations provide a model for microtia and auricle duplication. Development 140: 4386-4397.

55. Depew MJ, Simpson CA, Morasso M, Rubenstein JL (2005) Reassessing the Dlx code: the genetic regulation of branchial arch skeletal pattern and development. J Anat 207: 501-561.

56. Debiais-Thibaud M, Metcalfe CJ, Pollack J, Germon I, Ekker M, et al. (2013) Heterogeneous conservation of Dlx paralog co-expression in jawed vertebrates. PLoS One 8: e68182.

57. Takechi M, Adachi N, Hirai T, Kuratani S, Kuraku S (2013) The Dlx genes as clues to vertebrate genomics and craniofacial evolution. Semin Cell Dev Biol 24:

110-118.

58. Talbot JC, Johnson SL, Kimmel CB (2010) hand2 and Dlx genes specify dorsal, intermediate and ventral domains within zebrafish pharyngeal arches. Development 137: 2507-2517.

59. Thomas T, Kurihara H, Yamagishi H, Kurihara Y, Yazaki Y, et al. (1998) A signaling cascade involving endothelin-1, dHAND and msx1 regulates development of neural-crest-derived branchial arch mesenchyme. Development 125: 3005-3014.

60. Charite J, McFadden DG, Merlo G, Levi G, Clouthier DE, et al. (2001) Role of Dlx6 in regulation of an endothelin-1-dependent, dHAND branchial arch enhancer. Genes Dev 15: 3039-3049.

61. Barron F, Woods C, Kuhn K, Bishop J, Howard MJ, et al. (2011) Downregulation of Dlx5 and Dlx6 expression by Hand2 is essential for initiation of tongue morphogenesis. Development 138: 2249-2259.

62. Crump JG, Swartz ME, Eberhart JK, Kimmel CB (2006) Moz-dependent Hox expression controls segment-specific fate maps of skeletal precursors in the face. Development 133: 2661-2669.

63. Laurin M (1998) The importance of global parsimony and historical bias in understanding tetrapod evolution. Part II. Vertebral centrum, costal ventilation,

and paedomorphosis. Annales Des Sciences Naturelles-Zoologie Et Biologie Animale 19: 99-114.

64. Clack JA (2002) Patterns and processes in the early evolution of the tetrapod ear. J Neurobiol 53: 251-264.

65. Lombard RE, Bolt JR (1979) Evolution of the Tetrapod Ear - Analysis and Reinterpretation. Biological Journal of the Linnean Society 11: 19-76.

66. Clack JA (2002) Gaining ground : the origin and evolution of tetrapods. Bloomington, Ind.: Indiana University Press. viii, 369 p. p.

67. Laurin M (2010) How vertebrates left the water. Berkeley ; London: University of California Press. xv, 199 p. p.

68. Diogo R, Hinits Y, Hughes SM (2008) Development of mandibular, hyoid and hypobranchial muscles in the zebrafish: homologies and evolution of these muscles within bony fishes and tetrapods. BMC Dev Biol 8: 24.

69. Diogo R, Abdala V, Lonergan N, Wood BA (2008) From fish to modern humans--comparative anatomy, homologies and evolution of the head and neck musculature. J Anat 213: 391-424.

70. Parrington FR (1979) The evolution of the mammalian middle and outer ears: a personal review. Biol Rev Camb Philos Soc 54: 369-387.

71. Hildebrand M, Goslow GE (2001) Analysis of vertebrate structure. New York: Wiley. xiv, 635 p. p.

72. Gardner NM, Holliday CM, O'Keefe FR (2010) The Braincase of Youngina Capensis (Reptilia, Diapsida): New Insights from High-Resolution Ct Scanning of the Holotype. Palaeontologia Electronica 13.

73. Gaupp, E. Die Reichertsche theorie (Hammer,. Ambos-, und Kieferfrage). *Arch. Anat. Physiol. Suppl.*, 1-416 (1912).

74. Allin EF (1975) Evolution of the mammalian middle ear. J Morphol 147: 403-437.

75. Barghusen, H. R. in *The Ecology and Biology of Mammal-like Reptiles* (eds N. Hotton III, P. D. MacLean, J. J. Roth, & E. C. Roth) 253-262 (Smithsonian Institution Press, Washington, 1986).

76. Clouthier DE, Hosoda K, Richardson JA, Williams SC, Yanagisawa H, et al. (1998) Cranial and cardiac neural crest defects in endothelin-A receptor-deficient mice. Development 125: 813-824.

77. Yamada G, Mansouri A, Torres M, Stuart ET, Blum M, et al. (1995) Targeted mutation of the murine goosecoid gene results in craniofacial defects and neonatal death. Development 121: 2917-2922.

78. Tucker AS, Watson RP, Lettice LA, Yamada G, Hill RE (2004) Bapx1 regulates

patterning in the middle ear: altered regulatory role in the transition from the proximal jaw during vertebrate evolution. Development 131: 1235-1245.

79. Goodrich ES (1915) The chorda tympani and middle ear in reptiles, birds, and mammals. Quarterly Journal of Microscopical Science 61: 137-U114.

80. Westoll TS (1943) The hyomandibular of Eusthenopteron and the tetrapod middle ear. Proceedings of the Royal Society Series B-Biological Sciences 131: 393-414.

81. Thompson H, Tucker AS (2013) Dual origin of the epithelium of the mammalian middle ear. Science 339: 1453-1456.

82. Mallo M (2001) Formation of the middle ear: recent progress on the developmental and molecular mechanisms. Dev Biol 231: 410-419.

83. Romer AS, Price LI (1980) Review of the Pelycosauria. New York: Arno Press. x, 538 p., 523 leaves of plates p.

84. Gardner, N. M., Holliday, C. M. & O'Keefe, F. R. The Braincase of Youngina capensis (Reptilia, Diapsida): New Insights from High-Resolution CT Scanning of the Holotype. *Palaeontol. Electron.* **13**, 19A (2010).

85. Reisz, R. R. in *Major transitions in vertebrate evolution* (Indiana university press, Bloomington, 2007).

86. Westoll TS (1944) New light on the mammalian ear ossicles. Nature 154: 770-771.

87. Westoll TS (1945) The Mammalian Middle Ear. Nature 155: 114-115.